"This is an author-created, un-copyedited version of an article accepted for publication/published in Plasma Chemistry and Plasma Processing. Springer is not responsible for any errors or omissions in this version of the manuscript or any version derived from it. The Version of Record is available online at DOI: <a href="https://doi.org/10.1007/s11090-019-09981-w">https://doi.org/10.1007/s11090-019-09981-w</a>."

Formation of Nitrogen Oxides by Nanosecond Pulsed Plasma Discharges in Gas-Liquid Reactors

Robert J. Wandell, Huihui Wang, Radha K.M. Bulusu, Rachel O. Gallan, and Bruce R. Locke

Department of Chemical and Biomedical Engineering, FAMU-FSU College of Engineering, Florida State

University, Tallahassee, FL 32310-6046, United States

Corresponding author: Robert J. Wandell, <u>rjw05c@my.fsu.edu</u>, (850) 450-0904

#### **ABSTRACT**

A gas-liquid-film flow reactor with a nanosecond pulsed power supply was utilized to produce nitrogen oxides from Ar/N<sub>2</sub> mixtures (gas phase) and deionized water (liquid phase). Chemical analysis of the stable products found in both the gas and liquid phases was performed and chemical quenching was incorporated for the liquid phase samples in order to eliminate post plasma reactions. Significant amounts of NO and NO<sub>2</sub> in the gas phase and NO<sub>2</sub><sup>-</sup> and NO<sub>3</sub><sup>-</sup> in the liquid phase were determined using FTIR spectroscopy and ion chromatography, respectively. The production rate of all nitrogen oxides produced increased significantly with N<sub>2</sub> concentration while H<sub>2</sub>O<sub>2</sub> formation decreased slightly. The gas temperature of the plasma was approximately 525 K and was unaffected by N<sub>2</sub> concentration while the electron density ranged from 1x10<sup>17</sup> cm<sup>-3</sup> in pure Ar to 5.5x10<sup>17</sup> cm<sup>-3</sup> in 28% N<sub>2</sub>. The role of the •OH in the reaction pathway was assessed by adding CO as a gas phase radical scavenger showing that •OH is essential for conversion of the gas phase NO and NO<sub>2</sub> into water soluble NO<sub>2</sub><sup>-</sup> and NO<sub>3</sub><sup>-</sup>. Conversely, atomic oxygen originating from water is likely responsible for NO and NO<sub>2</sub> generation. Experiments with N<sub>2</sub>/O<sub>2</sub>/Ar mixtures and air showed a significant increase in NO<sub>2</sub> production caused by the additional generation of reactive oxygen species. An overall energy yield for all nitrogen oxides produced in the most efficient case was 50 eV/molecule.

#### **KEYWORDS**

Non-thermal plasma, Nitrogen fixation, Plasma activated water, Nanosecond discharge, Nitrogen oxides

## INTRODUCTION

1

The generation of nitrogen oxides (e.g., NO and NO<sub>2</sub>) from N<sub>2</sub> and O<sub>2</sub> in thermal and non-thermal plasma reactors has been extensively investigated over the last approximately 100 years [1-4]. In plasma reactors containing air or mixtures of nitrogen and oxygen, N<sub>2</sub> and O<sub>2</sub> react with plasma generated electrons in a number of different ways including direct dissociation and excitation, and typically the limiting step in the formation of higher oxides of nitrogen is the endothermic formation of nitric oxide, NO [1, 5]. While it has been found that vibrational excitation rather than thermal dissociation of N<sub>2</sub> can lead to a significant increase in the energy efficiency of NO formation, the energy efficiency of NO production with plasma is typically limited by the back reaction of NO with N atoms. Therefore, a quenching step utilizing steep cooling gradients with low pressure non-thermal microwave plasma has led to higher efficiency of NO synthesis from air [1, 6, 7]; however, the cost of such cooling and quenching steps needs further consideration and further oxidation of NO to higher oxides of nitrogen presents additional opportunities for improvements in nitrogen fixation efficiency.

On the other hand, over the last thirty years plasma reactors have also been extensively studied for the removal of nitrogen oxides from combustion and other gases for air pollution control [8-10] through direct and indirect reactions to form liquid soluble products such as nitrite (NO<sub>2</sub><sup>-</sup>) and nitrate (NO<sub>3</sub><sup>-</sup>) [11-25]. In dry gases, the removal of NO from combustion gas involves the oxidation of NO to NO<sub>2</sub>, and in both direct and indirect plasma, ozone, O<sub>3</sub>, may play an important role in this step [26-28]. The addition of catalysts and utilization of nanosecond pulses have also been found to enhance NO removal from exhaust gases [29-31]. The addition of water to the plasma leads to the formation of hydroxyl radicals (•OH) through water dissociation (and other reactions [32]) and these radicals lead to the formation of NO<sub>2</sub><sup>-</sup>, NO<sub>3</sub><sup>-</sup>, and peroxynitrite, ONOO<sup>-</sup>, causing significant decreases in pH due to the formation of the corresponding acids [33-37]. Water can be added in the form of vapor or as a mist, or the plasma can directly touch the liquid phase leading to water evaporating directly into the plasma [38-40]. Such low energy intensive chemical quenching provides an alternative method to produce higher oxides of nitrogen by rapid conversion of NO and NO<sub>2</sub> into products that are quickly absorbed into the liquid where they are less susceptible to degradation by the plasma and where reverse reactions are minimized.

In gas-liquid (argon-water) plasma high efficiency of hydrogen peroxide ( $H_2O_2$ ) has been demonstrated in a water spray plasma reactor [41, 42] and in a water film reactor [43], and combinations of  $H_2O_2$  and various nitrogen oxides are formed in air and  $N_2/O_2$  plasma contacting water [44]. Since  $H_2O_2$  and  $NO_3$  have very high Henry's Law constants, specifically in comparison to NO and  $NO_2$  [45], under atmospheric conditions the former two species are rapidly absorbed into the liquid phase; although some  $H_2O_2$  exists in the gas no HNO<sub>3</sub> is expected in the gas phase due to the rapid absorption.

Mixtures of such reactive oxygen species (ROS) (e.g., H<sub>2</sub>O<sub>2</sub> and •OH) and reactive nitrogen species (RNS) (e.g., NO, NO<sub>2</sub>-, NO<sub>3</sub>-, ONOO-) formed in plasma reactors with water and air (or mixtures with oxygen and nitrogen) have been termed "plasma activated water" (PAW) and have found recent applications and interests in medicine and agriculture [46-49]. For example, in agriculture the generation of nitrogen oxides with non-thermal plasma has been identified as a promising "green" alternative to the conventional Habor Bosch process [50, 51].

The reaction mechanisms and pathways of plasma nitrogen fixation of dry air and N<sub>2</sub>/O<sub>2</sub> mixtures [52] and gas-liquid systems [53, 54] including post plasma reactions [55] have been analyzed through kinetic modeling. Both

experiments and modeling have shown the importance of the post plasma reactions in PAW as well as the key peroxynitrite pathway in water [37, 56-58]. While the occurrence of the post-plasma peroxynitrite pathway has been proposed as a main reason for the relatively long-lasting antimicrobial properties of PAW, it also significantly complicates chemical analysis of plasma treated liquid water. This is particularly true for distinguishing reactions that occur in the plasma zone verses those that occur in the post-plasma reactions.

The present study utilizes a continuously flowing gas/liquid plasma reactor where the liquid and gas phases exit the system after plasma treatment upon which immediate chemical quenching can be incorporated to eliminate post-plasma reactions in the liquid effluent, and the gas and liquid products can be quickly and directly determined. The gas phase was analyzed using a FTIR flow cell immediately following the plasma reactor and the chemically quenched liquid samples were analyzed with ion chromatography. This work reports the formation of the stable gas and liquid phase products generated by the non-thermal plasma contacting with liquid water with nitrogen present before post-plasma reactions take place to allow for assessment of the products generated by the plasma discharge alone. Mixtures of N<sub>2</sub>/Ar and N<sub>2</sub>/Ar/O<sub>2</sub> were utilized in the feed gas to assess the role of reactive oxygen species verses •OH in the reaction pathway and carbon monoxide (CO) was used as an •OH scavenger to determine gas phase production of this species [59].

#### **EXPERIMENTAL METHODS**

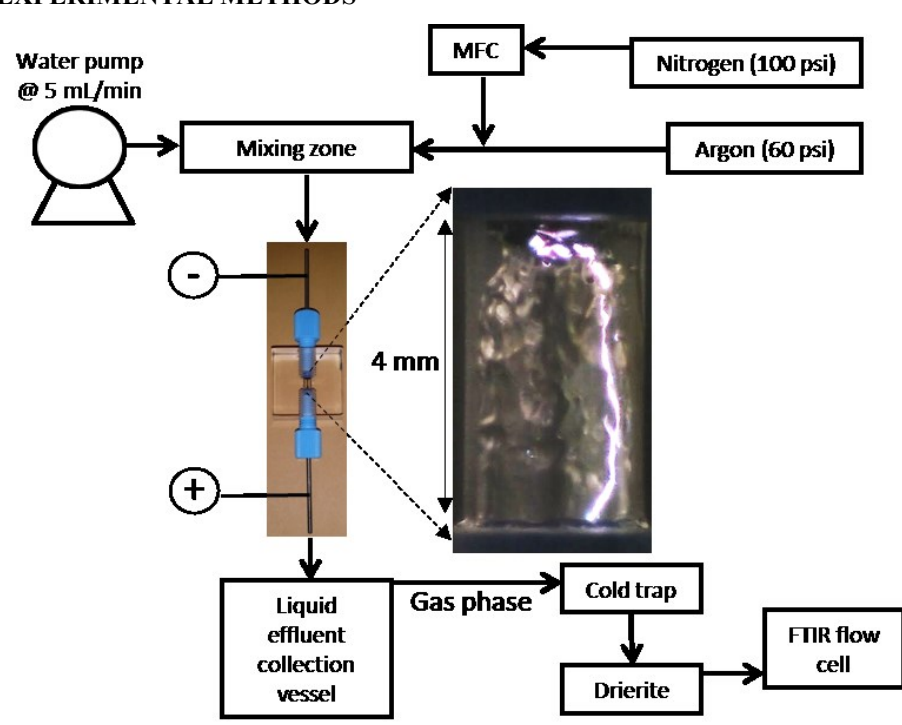


**Fig. 1** Process schematic of the experimental setup used in this study. Photo taken at 1/8000 s exposure shows one plasma channel propagating along the gas/liquid interface.

A process schematic for the experimental setup used in this study is shown in Figure 1. Liquid water, delivered at 5 mL/min by a high-pressure reciprocating pump, was mixed with argon (414 kPa, 60 psig) in a mixing

zone (1.6 mm Swagelok tee joint) before entering the inlet of the plasma reactor (0.5 mm ID stainless-steel capillary). The small inner diameter of the inlet capillary limited the total gas flow into the reactor to 3.4 L/min. With this setup the residence times for the liquid and gas were 127 ms and 4 ms, respectively [60]. A mass flow controller (Brooks, 5850E) was used to add  $N_2$  to Ar in order to achieve various  $N_2$ /Ar concentrations while maintaining a constant total gas flow rate. A second mass flow controller was employed in experiments where CO or  $O_2$  were added to the  $N_2$  and Ar mixture.

When the gas/liquid mixture enters the discharge region of the reactor a flowing liquid film is formed along the inner walls of the tube and is accompanied by a gas phase flowing though the central core [60]. The stainless-steel inlet and outlet capillaries of the plasma reactor also function as the anode and cathode, respectively. A nanosecond power supply (Eagle Harbor Technologies, Inc.) was connected across the electrodes to produce a filamentary plasma channel which propagates along the interface of the liquid film. The same output settings on the power supply were used for all experiments in this work; 16 kV, 40 ns, 10 kHz. Due to the very short residence times of the gas and liquid phases in the reactor, the reactor quickly reaches steady state after the plasma is turned on. Based on the liquid/gas residence times and the pulse frequency (10 kHz), 1270 pulses occur during the residence time of the liquid (127 ms) while 40 occur for the gas phase (4 ms).

After exiting the plasma reactor, the liquid phase was collected in a sampling vessel while the gas phase flowed directly to an FTIR spectrometer (Jasco - 6700) equipped with a 5 m gas flow cell. Prior to entering the flow cell, the gas phase passed through a dry-ice/acetone cold trap followed by a DIERITE® packed bed to remove remaining water which due to its large dipole moment causes significant interference with the FTIR measurement. For experiments where CO was used, the CO<sub>2</sub> concentration in the gas phase effluent was also quantified using FTIR. More details on the gas phase measurement including sample spectra can be found in the Appendix.

The NO<sub>2</sub><sup>-</sup> and NO<sub>3</sub><sup>-</sup> in the liquid phase of the effluent were analyzed using ion chromatography (Dionex, Aquion). Due to the occurrence of post-plasma reactions between H<sub>2</sub>O<sub>2</sub> and NO<sub>2</sub><sup>-</sup>, the liquid phase of the effluent was discharged into a solution of NaOH to slow down the reaction rate of the peroxynitrite reaction pathway for accurate quantification of the concentrations exiting the reactor [58]. For H<sub>2</sub>O<sub>2</sub> measurements, the effluent was discharged into a sodium azide solution to rapidly remove NO<sub>2</sub><sup>-</sup> from the solution before quantification with the TiSO<sub>4</sub> colorimetric method using a UV-Vis spectrometer (PerkinElmer, Lambda 35) [58, 61]. The conductivity and pH were determined in separate samples without the addition of NaOH or sodium azide. More details on the liquid phase measurement can be found in the Appendix.

Voltage and current were measured with an oscilloscope (Tekronix MDO 3014; Beaverton, OR) equipped with two high voltage probes (TektronixP6015A, 1/1000; Beaverton, OR) in conjunction with a Rogowski coil (Pearson Electronics, model 6585; Palo Alto, CA). Energy per pulse was determined by integrating the instantaneous power (VxI) across the entire pulse as in Equation 1.

Energy per pulse =  $\int (V \times I)dt$  E1

V: Instantaneous voltage

I: Instantaneous current

## t: Time

The energy yield for chemical species produced was determined by dividing the average discharge power by the rate of production. More details on the electrical measurement including temporal probe alignment can be found in the Appendix as well as in previous publications using the same system [60, 62].

Time averaged electron density and gas temperature of the plasma were estimated using optical emission spectroscopy (Avantes, AvaSpec-ULS3848; wavelength range: 300-403 nm for gas temperature, 600-700 nm for electron density). For  $N_2$  concentrations less than 5%, gas temperature was determined using •OH (A-X) from 305-320 nm using the same method from our previous work, i.e. two temperature fitting of the Boltzmann plot obtained using MassiveOES [62-65]. For higher concentrations of  $N_2$ , the gas temperature was determined with the  $N_2$  (C-B) at 337 nm following the fitting protocol in Vorac et al. using MassiveOES [64, 65]. Electron density was estimated using Stark broadening of the  $H_\alpha$  peak at 656.3 nm using two-Voigt function. More details of this measurement can be found in the Appendix as well as our previous work [62, 63, 66, 67].

All measurements were repeated in triplicate and the error bars found throughout this manuscript represent plus and minus one standard deviation from the mean.

#### RESULTS AND DISCUSSION

The focus of this work is chemical species analysis, however, for assessment and comparison of chemical species generation in this plasma system to other plasma and non-plasma processes, measurement of the electrical and plasma properties as well as visual observations of the plasma are essential.

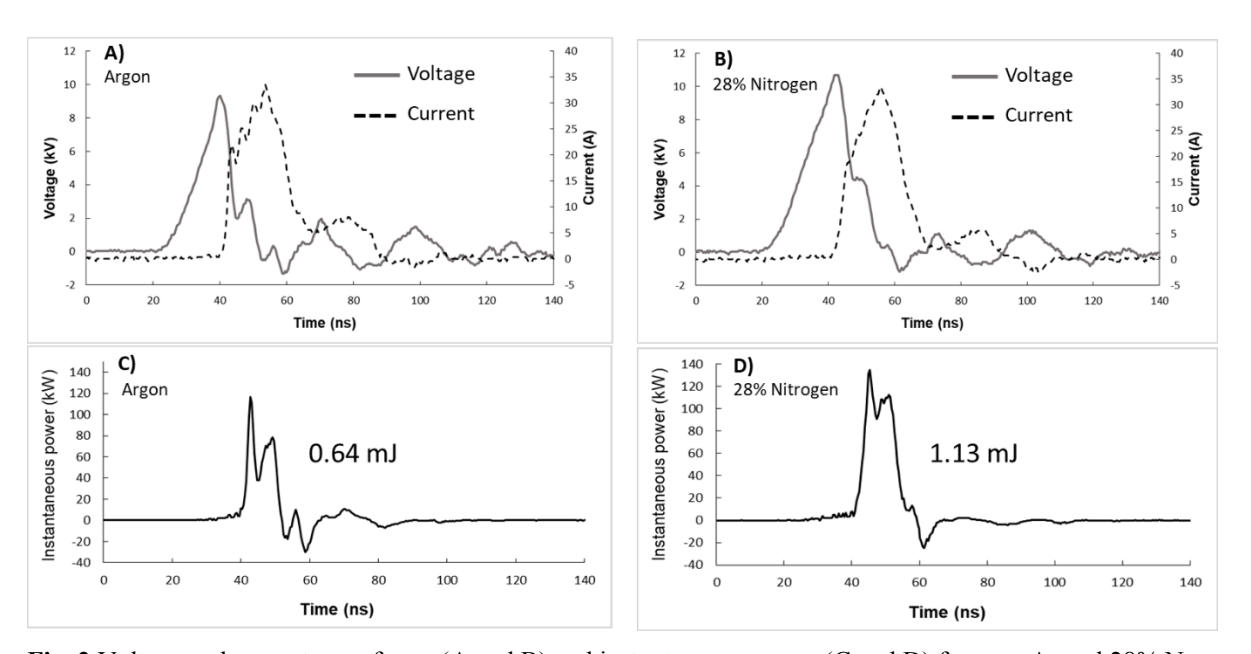


Fig. 2 Voltage and current waveforms (A and B) and instantaneous power (C and D) for pure Ar and 28% N<sub>2</sub>

Table 1 Electrical measures for various concentrations of nitrogen in argon

Nitrogen (%)	Energy per pulse (mJ)	Peak voltage (kV)	Peak curret (A)	Average discharge power (W)
0.00	0.64	9.83	33.47	6.37
0.06	0.76	9.20	32.40	7.59
0.71	0.75	8.87	32.00	7.48
1.77	0.78	9.61	32.67	7.82
3.55	0.82	9.16	31.87	8.21
7.10	0.84	9.40	32.00	8.39
14.19	1.08	9.83	31.33	10.76
21.29	1.08	10.73	33.07	10.76
28.39	1.13	10.81	33.07	11.35

Figure 2 and Table 1 show the electrical properties of the discharge for various concentrations of  $N_2$  in Ar. At 28%  $N_2$  the total energy dissipated per pulse increased by approximately a factor of 2 when compared to pure Ar. The peak current was unaffected by increasing  $N_2$  and the peak voltage (breakdown voltage) increased by 10%. The increase in breakdown voltage is consistent with Paschen's law where the breakdown voltage for  $N_2$  is higher than argon [68]. The slight increase in breakdown voltage provides one cause of the significant increase in total energy. When the instantaneous powers  $(I^*V)$  for pure Ar and the 28%  $N_2$  mixture are compared (C and D of Figure 2) it also appears that the pulse duration is slightly longer with  $N_2$  added and this also contributes to the higher energy per pulse. No significant changes of the voltage and current were found with the addition of  $O_2$  or  $O_2$  at the concentrations utilized, 0-15% and 0-5%, respectively.

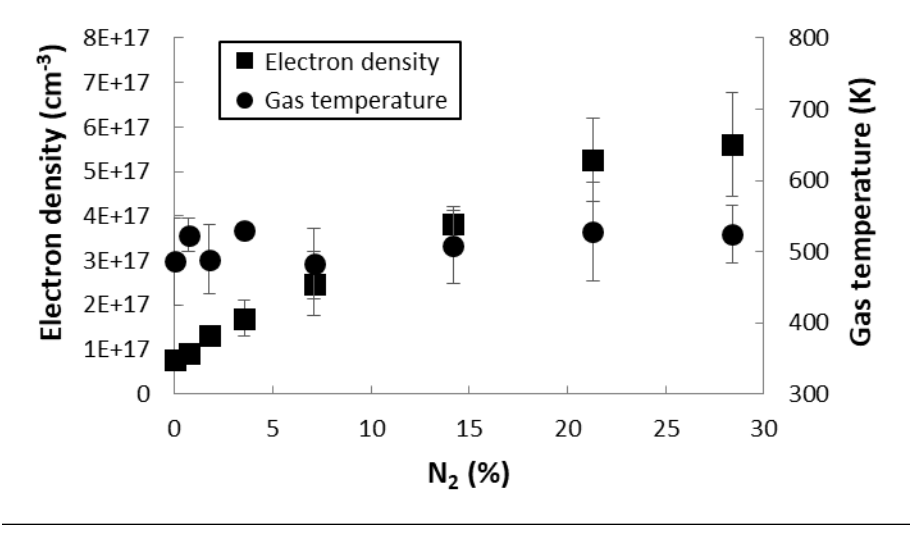


Fig. 3 Gas temperature and electron density as a function of nitrogen concentration

The electron density and gas temperature for the plasma discharge are shown in Figure 3 for various concentrations of  $N_2$  in Ar. The gas temperature was found to be approximately 525 K and was unaffected by the  $N_2$  concentration. A linear increase in electron density was found with increasing  $N_2$  concentration. With no  $N_2$  present the electron density was  $1x10^{17}$  cm<sup>-3</sup> while at 28%  $N_2$  the electron density increased to  $5.5x10^{17}$  cm<sup>-3</sup>. OES

measurements were not performed for the experiments with the addition of  $O_2$  or CO, however, because no change in discharge power was observed at the relatively low concentrations utilized, little to no change is also expected in the plasma properties.

To further investigate the lack of significant change in the plasma gas temperature with  $N_2$  concentration while the electron density increased by almost one order of magnitude, the diameter of the plasma channel was estimated. The flux of electrons (current) though a radial cross-section of the plasma channel was utilized to estimate the diameter, and the volume of the generated plasma channels based on the measured variables was determined by Equation 2 [66].

$$V_p = \frac{I_d L^2}{n_e e \mu_e V_d}$$
 E2

*I<sub>d</sub>*: Discharge current, 33 A (no change)

e: Elementary electron charge, 1.602\*10<sup>-19</sup> C (constant)

V<sub>d</sub>: Discharge voltage, 9.8 kV@0%, 10.1 kV@28%

L: Gap distance 0.4 cm, (constant)

 $n_e$ : Electron density 7.8\*10<sup>16</sup> cm<sup>-3</sup> @0%, 5.6\*10<sup>17</sup> cm<sup>-3</sup> @28%

 $\mu_e(T_p)$ : Electron mobility 245 cm<sup>2</sup>/V/s (no change)

 $V_p$ : Plasma channel volume 0.18 mm<sup>3</sup> @0%, 0.22 mm<sup>3</sup> @28%

 $I_d$  and  $V_d$  were obtained from electrical measurements and  $n_e$  from optical emissions. The electron mobility was determined by solving the Boltzmann equation using BOLSIG+ with the plasma temperatures estimated from OES and an estimation of the reduced electric field for parallel plate geometry  $(V_d/L)$  [69]. The length of the plasma channel was assumed to be equal to the electrode gap distance (4 mm).

The plasma volume in pure argon was estimated using E2 to be  $0.18 \text{ mm}^3$  corresponding to a plasma diameter of 0.24 mm. When  $28\% \text{ N}_2$  was added to the feed gas, the estimated plasma volume decreased to  $0.02 \text{ mm}^3$ , corresponding to a diameter of 0.08 mm.

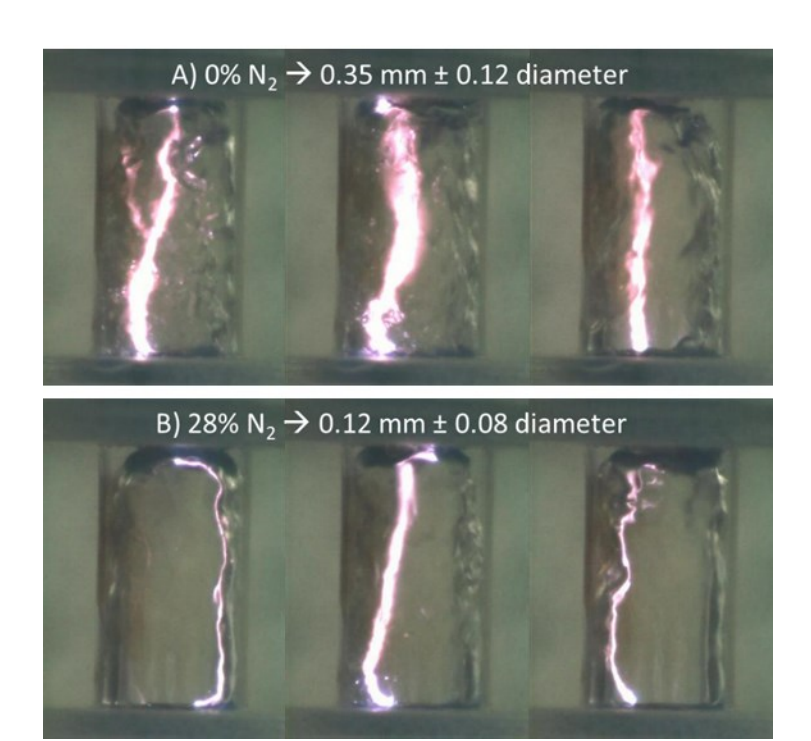


Fig. 4 Various images of a single discharge channel propagating along the gas-liquid interface. Images were taken with a 1/8000 sec shutter speed. Plasma diameter was estimated by the software integrated measurement tool (Keyence, VW-9000). The diameters reported represent the average and standard deviation of the images shown. A) Argon carrier gas, diameter -0.35 mm  $\pm 0.12$  B) 28% N<sub>2</sub> in argon, diameter  $-0.12 \pm 0.08$ .

The decrease in plasma diameter with increasing N<sub>2</sub> concentration estimated by the current density relation, E2, was confirmed by measurements taken with high speed imaging shown in Figure X. Further, the measured values of the plasma diameter found with imaging match well with the current density estimates.

From these estimates of plasma volume and electron density, the total number of free electrons can be calculated as a function of nitrogen concentration. Due to the increase in electron density corresponding with a decrease in plasma volume, the total number of electrons remains relatively unchanged when comparing the pure argon case  $(1.4 \times 10^{13})$  total electrons to  $28\% N_2 (1.3 \times 10^{13})$ .

Based on the above assessment of the electrical and plasma properties as well as the photograph shown in Figure 4, the plasma is best described as a filamentary non-thermal plasma channel generated in the gas phase which propagates along the liquid interface [60]. This system is similar to that of a transient spark discharge [70-73]. The plasma generated transient spark discharges are also short-lived filamentary plasma channels (streamers) with an electron density on the same order of magnitude as that found in this study. The energy dissipated per pulse is also similar ( $\approx$ 1 mJ). The transient spark discharge with dry air reports significant NO and NO<sub>2</sub> generation and when a water spray was introduced to the transient spark nitrates and nitrites were also produced. A comparison for NOx generation with transient spark discharges to this work is provided in Table 2.

#### Potential chemical reactions

NO formation in thermal plasmas as well as in combustion processes has been well studied where the generally accepted reaction pathway is the Zeldovich mechanism. In this reaction pathway NO is formed through thermal dissociation of O<sub>2</sub> and N<sub>2</sub> where the high bond strength of N<sub>2</sub> causes the N<sub>2</sub> dissociation to be the rate limiting step [1]. NO production from dry air and non-thermal plasma, where the gas temperature is not high enough for thermal dissociation to dominate (<5500 K), is initiated through electron impact dissociation and excitation of O2 (R2) and N2 (R1) which generate atomic oxygen and various excited states of N2. The vibrational excitation of N<sub>2</sub> lowers the bond strength of the molecule and allows for NO generation in non-thermal conditions through reactions with atomic oxygen (R3). Additional NO generation can then also be achieved through Reaction 4.

$$N_{2} + e^{-} \rightarrow N_{2}^{*} + e^{-}$$

$$O_{2} + e^{-} \rightarrow O + O + e^{-}$$

$$O + N_{2}^{*} \rightarrow NO + N^{*}$$

$$R3$$

$$N^{*} + O_{2} \rightarrow NO + O$$

$$R4$$

This pathway is known as the Zeldovich mechanism stimulated by vibrational excitation [1]. Further oxidation of NO into NO<sub>2</sub> can then be achieved by additional reactions with atomic oxygen and ozone (R5 and R6).

NO + O + 
$$\rightarrow$$
 NO<sub>2</sub> 3E-11  $\frac{cm^2}{mol.s}$  R5  
NO + O<sub>3</sub>  $\rightarrow$  O<sub>2</sub> + NO<sub>2</sub> 1.8E-14  $\frac{cm^2}{mol.s}$  R6

$$NO + O_3 \rightarrow O_2 + NO_2$$
 1.8E-14  $\frac{cm^s}{mol.s}$  R6

Once formed, the gas phase NO and NO<sub>2</sub> can be converted into NO<sub>2</sub> and NO<sub>3</sub> with the addition of liquid water (R7 and R8). However, solubility of these gasses in water as well as mass transfer resistance limits rapid conversion in this manner.

$$NO_{2(aq)} + NO_{2(aq)} + H_2O \rightarrow NO_2^- + NO_3^- + 2H^+$$
 R7

$$NO_{(aq)} + NO_{2(aq)} + H_2O \rightarrow 2NO_2^- + 2H^+$$
 R8

When water vapor is present in a non-thermal plasma system, •OH is formed in abundance through election impact with water molecules in the plasma channel (R9). In cases with high •OH concentrations, typically with liquid water contacting the plasma, •OH can combine to form hydrogen peroxide (H<sub>2</sub>O<sub>2</sub>) (R10) which can then be sequestered in the liquid as a stable product [74]. Alternatively, the •OH can react to form water and atomic oxygen (R11) which could provide an additional source of the atomic oxygen needed for NO production.

$$H_2O + e^- \rightarrow \bullet H + \bullet OH + e^-$$
 R9

•OH + •OH 
$$\rightarrow$$
 H<sub>2</sub>O<sub>2</sub> 2.6E-11  $\frac{cm^3}{mol.s}$  R10

•OH + •OH 
$$\rightarrow$$
 H<sub>2</sub>O + O 1.5E-12  $\frac{cm^3}{mol.s}$  R11

An alternate pathway for NO generation when water is present is by the reaction of •OH with atomic nitrogen (R12). Direct conversion of NO into HNO<sub>2</sub> can also be achieved through reaction with •OH as well as conversion of NO<sub>2</sub> into HNO<sub>3</sub> (R13 and R14). Due to their high rate constants, Reactions 13 and 14 likely play key roles in the generation of water-soluble nitrogen oxides when water is present in non-thermal plasmas. This is analogous to hydrogen peroxide generation where once the product is sequestered into the liquid it is less likely to be degraded by the plasma.

$$N + \bullet OH \rightarrow NO + H$$
 5E-11  $\frac{cm^3}{mol.s}$  R12  
 $NO + \bullet OH \rightarrow HNO_2$  3E-11  $\frac{cm^3}{mol.s}$  R13  
 $NO_2 + \bullet OH \rightarrow HNO_3$  3E-11  $\frac{cm^3}{mol.s}$  R14

# Gas phase analysis

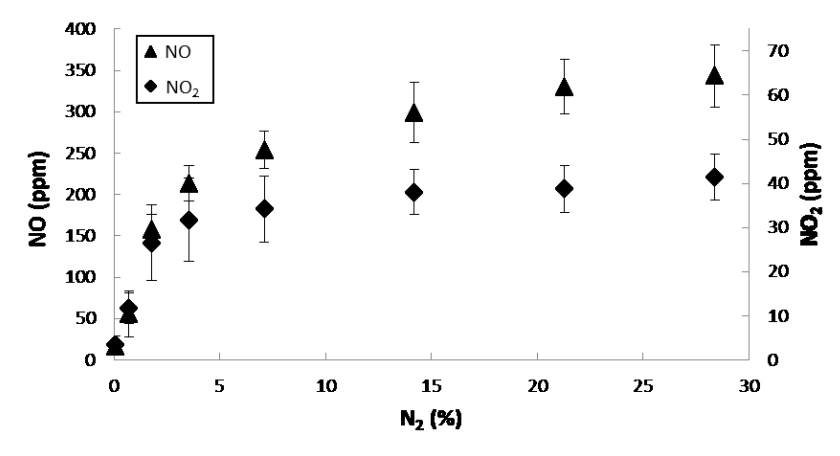


Fig. 5 Gas phase analysis for various N<sub>2</sub>/Ar concentrations

Figure 5 shows the concentrations of NO and NO<sub>2</sub> in the gas effluent of the reactor for various N<sub>2</sub>/Ar concentrations. Both NO and NO<sub>2</sub> production increase sharply with nitrogen concentration up to 5%. At higher concentrations, NO<sub>2</sub> production levels off while NO production shows a gradual increase. Significantly less NO<sub>2</sub> is produced compared to NO at all N<sub>2</sub>/Ar concentrations investigated. This could be explained by NO<sub>2</sub> being a secondary reaction product, NO must first be formed through Reaction 3 followed by an additional reaction with atomic oxygen (R5) to form NO<sub>2</sub>. Another consideration is that the reaction rate of O with N<sub>2</sub>\* to form NO (R3) is faster than that of O with NO to form NO<sub>2</sub> (R5). The leveling off of NO<sub>2</sub> implies that there is an atomic oxygen limitation at higher N<sub>2</sub> concentrations. The leveling off of NO also suggests a limitation on the availability of atomic oxygen, although another possibility is a limitation in •OH since NO can be directly formed from •OH and N

(R12). Because no  $O_2$  was present in the feed for these experiments a likely source of atomic oxygen is from water via Reaction 11, this is supported by modeling work with underwater discharges [75, 76]. Reactions 15 and 16 are also potential pathways for O production from water by direct electron collisions and electronically excited water,  $H_2O^*$ , respectively.

$$H_2O + e^- \rightarrow 2H^{\bullet} + O + e^-$$
 R15  
 $H_2O^* + H_2O \rightarrow H_2 + O + H_2O$  R16

While no chemical probes for atomic oxygen were employed in this study, confirmation of the presence of this short-lived species was found with optical emission spectroscopy (777 nm). A sample spectrum showing the presence of this band is given in the Appendix (Figure 17). Further experimental and modeling studies are needed to assess the most predominant pathway(s) for O production in this system.

# Liquid phase analysis

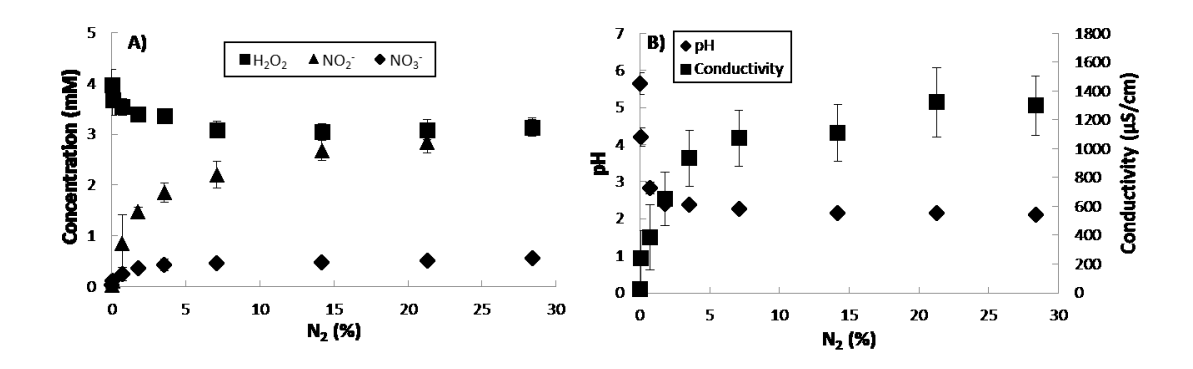


Fig. 6 Liquid phase analysis for various  $N_2/Ar$  concentrations. A) – Concentrations of stable chemical species produced B) – pH and conductivity of effluent

Figure 6 shows the liquid phase products for the various N<sub>2</sub>/Ar mixtures. For pure Ar the only stable product found in the liquid phase was H<sub>2</sub>O<sub>2</sub> [74]. When only a small amount of N<sub>2</sub> was added (550 ppm) NO<sub>2</sub><sup>-</sup> and NO<sub>3</sub><sup>-</sup> were detected in the liquid. As the N<sub>2</sub> concentration increased, the NO<sub>2</sub><sup>-</sup> and NO<sub>3</sub><sup>-</sup> in the liquid phase increased following the same trends as NO and NO<sub>2</sub> in the gas phase, respectively. This implies that the NO<sub>2</sub><sup>-</sup> and NO<sub>3</sub><sup>-</sup> measured at the exit of the reactor are formed directly from the reactions of •OH with gas phase NO and NO<sub>2</sub> (R13 and R14). The decrease in H<sub>2</sub>O<sub>2</sub> with increasing N<sub>2</sub> also supports this hypothesis due to •OH radical scavenging by NO and NO<sub>2</sub> in the gas phase. Here, the drop in H<sub>2</sub>O<sub>2</sub> cannot be attributed to post plasma reactions with NO<sub>2</sub><sup>-</sup> because the NO<sub>2</sub><sup>-</sup> was removed with sodium azide immediately after exiting the reactor. Additional support can also be seen in the significant drop of pH in the liquid effluent as the NO<sub>2</sub><sup>-</sup> and NO<sub>3</sub><sup>-</sup> concentrations increase. For these reasons the NO<sub>2</sub><sup>-</sup> and NO<sub>3</sub><sup>-</sup> detected in the liquid are assumed to be in the form of HNO<sub>2</sub> and HNO<sub>3</sub>. The

simultaneous increase of conductivity and decrease in pH can be correlated to increases of HNO<sub>3</sub> and HNO<sub>2</sub> as shown in Figure 7.

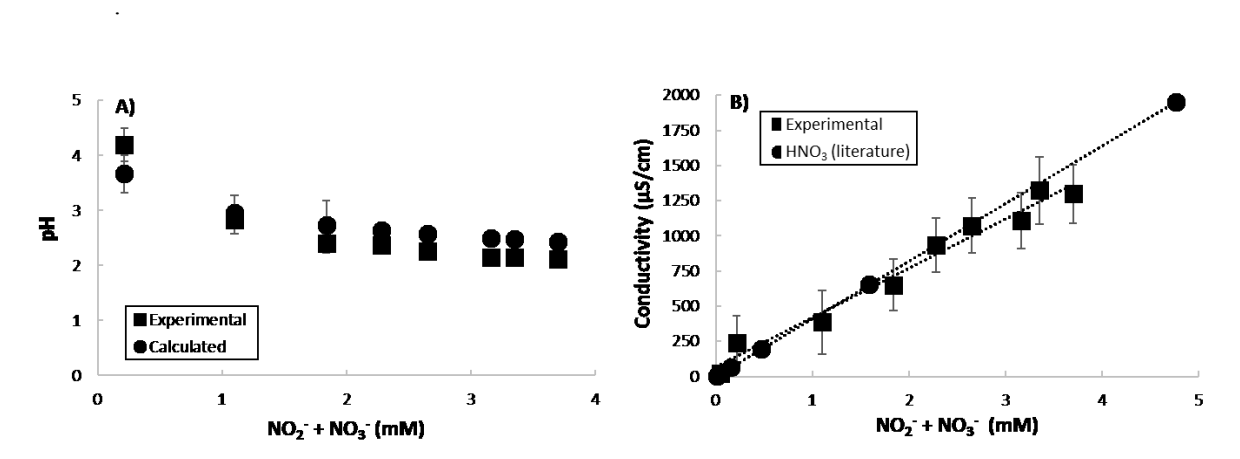


Fig. 7 A) – Comparison of the measured pH of the PAW effluent as a function of nitrite and nitrate concentrations against the calculated pH if it is assumed all  $NO_2^-$  and  $NO_3^-$  are in the form of  $HNO_2$  and  $HNO_3$ . B) - Comparison of the measured conductivity of the PAW effluent as a function of nitrite plus nitrate concentrations against literature values for the conductivity of various  $HNO_3$  solutions [77].

It should again be noted that if the liquid phase was not quenched at the exit of the reactor, more  $NO_3^-$  would be formed in post plasma reactions between  $NO_2^-$  and  $H_2O_2$  through the peroxynitrite pathway where after a sufficient period of time all  $NO_2^-$  would be converted into  $NO_3^-$ . Because the peroxynitrite pathway occurs on the time scale of minutes to hours depending on the concentration and pH of the plasma activated water, and the average liquid residence time in the reactor is only 127 ms, this pathway can be considered to have a negligible effect on the reactions occurring in the plasma reactor assessed in the present study [58].

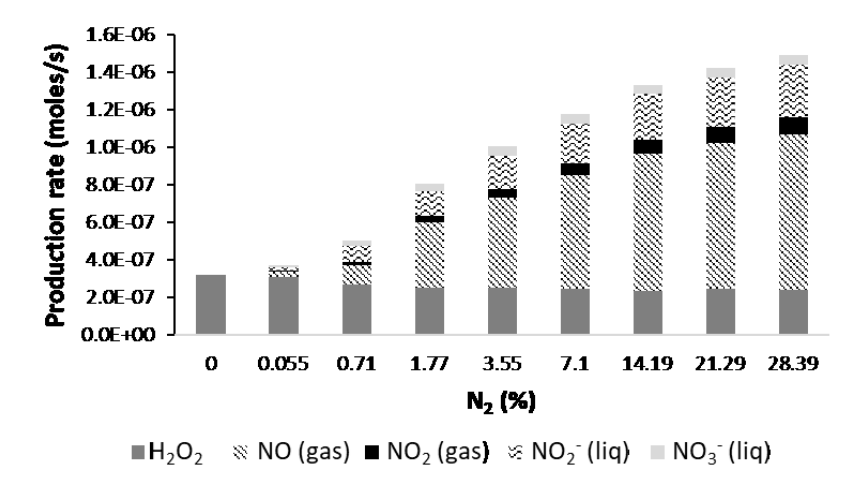


Fig. 8 Production rates of all measured species in the liquid and gas phases as a function of  $N_2$  percentage in feed gas.

Figure 8 shows the rates of production of all the major chemical species produced in the N<sub>2</sub>/Ar mixtures. Most nitrogen products detected exist in the gas phase and account for over 80% of all nitrogen oxide species, the majority of which are in the form of NO. High concentrations of H<sub>2</sub>O<sub>2</sub> are also produced despite the likelihood that a limitation in •OH is responsible for the lack of conversation of NO and NO<sub>2</sub> into HNO<sub>2</sub> and HNO<sub>3</sub>, respectively. This result is consistent with previous analysis of this reactor system that utilized gas and liquid phase radical scavengers to show that H<sub>2</sub>O<sub>2</sub> was generated from •OH near the gas-liquid interface and that H<sub>2</sub>O<sub>2</sub> was not strongly affected by •OH scavenging in the gas phase [78].

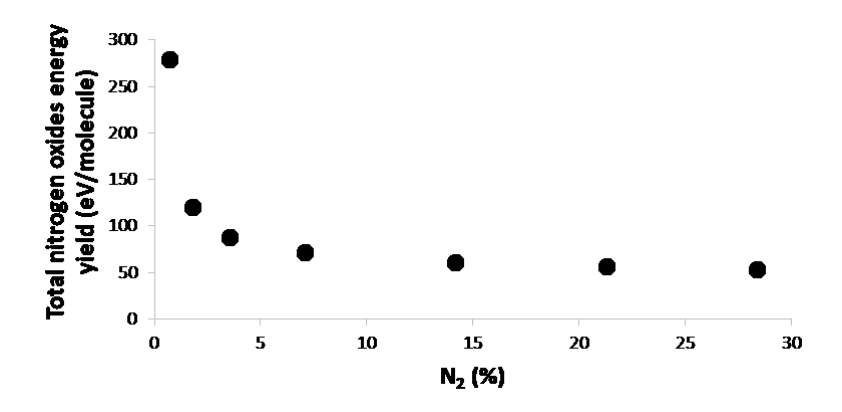


Fig. 9 Energy yield for total nitrogen oxides produced in both the liquid and gas phases as a function  $N_2/Ar$  concentration.

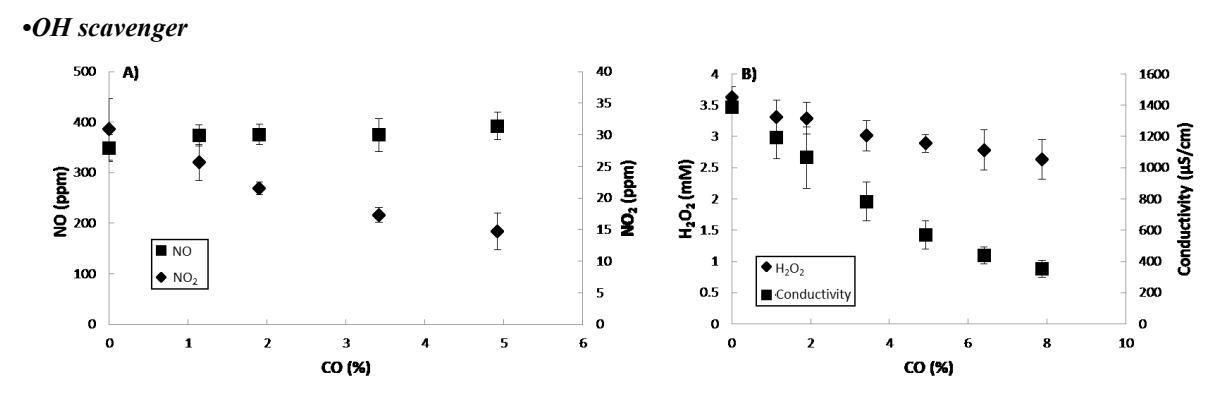
The energy yield for total nitrogen oxides produced is shown in Figure 9 as a function of  $N_2$  concentration. From Figure 9 the energy cost per molecule decreases as the  $N_2$  concentration increased up to 10% after which it levels off at approximately 50 eV/molecule. Table 2 provides a comparison of the energy yield of this study to other plasma processes.

Table 2 Energy yield comparison for other plasma systems

Process	Product	Feed	Conditions	Energy yield	Energy yield	Reference
				Moles/J	eV/molecule	
Birkeland and Eyde	NO	N <sub>2</sub> , O <sub>2</sub>	thermal plasma arc	4.1E-07	2.5E+01	cited in [1]
Birkeland and Eyde	NO	N <sub>2</sub> , O <sub>2</sub>	thermal plasma arc	5.6E-07	1.9E+01	cited in [79]
Birkeland and Eyde	NO	N <sub>2</sub> , O <sub>2</sub>	thermal plasma arc	8.7E-07	1.2E+01	cited in [80]
Thermal plasma	NO	N <sub>2</sub> , O <sub>2</sub>	20-30 atm, 3000-3500 K	1.2E-06	9.0E+00	cited in 1[1]
Microwave	NO	N <sub>2</sub> , O <sub>2</sub>	magnetic field	3.5E-06	3.0E+00	cited in 1 [1]

non thermal plasma			and cooled walls			
Low pressure	NO	N <sub>2</sub> , O <sub>2</sub>	with catalyst	1.2E-06	8.7E+00	Mutel, cited in [81]
Plasma jet	NO	N <sub>2</sub> , O <sub>2</sub>	varied O <sub>2</sub> /N <sub>2</sub> ratio	4.6E-07	2.3E+01	Krop/Pollo, cited in [81]
Plasma jet	NO	air	3.5 W plasma jet	9.5E-10	1.1E+04	[82]
Rotating disk with injected water	NO	air		3.1E-07	3.3E+01	Krop/Pollo, cited in [81]
Plasma beam	NO	air	30 kW	1.0E-06	1.0E+01	Alekesev, cited in [81]
Jet arc	NO			2.8E-07	3.7E+01	Coudert, cited in [81]
Plasmatron gliding arc	NO <sub>3</sub> -	air with water	240 W	3.4E-09	3.1E+03	[83]
Glow discharge	NO <sub>3</sub> -		420 W 162 MHz	1.8E-09	5.7E+03	[79]
AC gliding arc over water	NO <sub>3</sub> -	air with water	2 electrodes 300 W	2.9E-08	3.6E+02	[44]
AC gliding arc over water	NO <sub>3</sub> -	air with water	3 electrodes 600 W	2.4E-08	4.3E+02	[44]
AC gliding arc with spray	NO <sub>3</sub> -	air with water	3 electrodes 600 W with spray	5.3E-09	2.0E+03	[44]
Bubbling in water	HNO <sub>3</sub>	air with water	underwater pulsed discharge with bubbles	5.4E-09	1.9E+03	[44]
Transient spark	NOx	Dry air	Transient spark, DC self- pulsing	1.2E-7	9.0E+1	[70]
Transient spark	NO <sub>x</sub> , NO <sub>2</sub> -, NO <sub>3</sub> -	air with water	Transient spark with electrospray	1.1E-7	9.6E+1	[73]

The formation of nitric oxide, NO, is a long studied reaction in plasma chemistry due to its importance in fertilizer formation. For example, in 1900 Birkeland and Eyde developed a thermal plasma arc furnace which was used commercially to make NO from N<sub>2</sub> and O<sub>2</sub>. The thermodynamic limit for this reaction is 1 eV/molecule and the efficiency reported by Birkeland and Eyde was 25 eV/molecule [1]. The highest efficiency for nitrogen fixation with a plasma process was a non-thermal microwave plasma with magnetic field and low pressure (3 eV/mol) however, the cost of attaining the low pressure and the magnetic field were not included [1]. Of the various plasma process listed in Table 2 the transient spark [70-72] has the most closely related plasma properties to this work and the energy yield for total NO<sub>X</sub> (NO/NO<sub>2</sub>) from air is similar in magnitude to that reported in this study. When an electrospray was combined with the transient spark, nitrate and nitrite were observed in the exiting liquid, however the energy yield for total nitrogen oxides remained similar [73]. It is important to note that the plasma reactor utilized in this work only requires air and water feed and operates at near atmospheric conditions.



**Fig. 10** Chemical analysis of the gas phase (left) and liquid phase (right) for various concentrations of carbon monoxide added to a  $28\% \text{ N}_2/\text{Ar}$  mixture. Conductivity was used as an indicator of changes in  $\text{NO}_2^-$  and  $\text{NO}_3^-$  in the liquid phase.

To further investigate the role of •OH in the process, CO was added to the gas phase (0-5%) of the 28%  $N_2$ /Ar mixture. CO is an excellent gas phase •OH scavenger and due to the fast rate of reaction between •OH and CO (R15), CO added to the gas phase will rapidly react with •OH radicals and prevent them from participating in reactions with other compounds [78, 84]. The effectiveness of CO as a gas phase •OH scavenger is illustrated in Figure 10 where the •OH consumed in CO<sub>2</sub> production by Reaction 17 increases with CO% added to the gas feed.

$$CO + \bullet OH \rightarrow CO_2 + H$$
 1.87E-13  $\frac{cm^2}{mol. s}$  R17

For the data shown in Figure 10, conductivity was used as an indicator of changes in NO<sub>2</sub><sup>-</sup> and NO<sub>3</sub><sup>-</sup> in the liquid phase. The addition of CO decreased the production of NO<sub>2</sub>, NO<sub>2</sub><sup>-</sup>, NO<sub>3</sub><sup>-</sup>, and H<sub>2</sub>O<sub>2</sub> significantly but had little effect on NO. This result clearly indicates that direct •OH reactions play important roles in NO<sub>2</sub>, NO<sub>2</sub><sup>-</sup>, and NO<sub>3</sub><sup>-</sup> generation, and may not directly react with N via Reaction 12 to a significant degree. With no O<sub>2</sub> present in the feed gas, a reduction in the •OH concentration will also cause a reduction in the atomic oxygen formed by Reaction 11. Because there are no possible reactions of •OH to form NO<sub>2</sub>, the reduction in NO<sub>2</sub> formation is likely caused by the reduction in availability of atomic oxygen. However, a chemical probe specific to atomic oxygen would be useful to confirm this finding. Since reactions with atomic oxygen are also probable pathways for NO generation, the lack of any significant change in NO concentration is possibly due to a decrease in NO production (R3) being balanced by a decrease in consumption (conversion to NO<sub>2</sub>), (R5).

The lower limit on the production of •OH when no N<sub>2</sub> was present in the feed can be estimated based on the conversion of CO to CO<sub>2</sub> (R17) and H<sub>2</sub>O<sub>2</sub> formation (R10). Based on these reactions, for every mole of CO<sub>2</sub> produced one mole of •OH is consumed while for every mole of H<sub>2</sub>O<sub>2</sub> produced two moles of •OH are consumed. Additionally, the •OH consumed in the generation of nitrogen oxides was estimated by assuming that all NO and NO<sub>2</sub> are produced by reactions with atomic oxygen (R3 and R5) and that the atomic oxygen is produced by Reaction

11. Thus, for every mole of NO produced two moles of •OH are consumed, and for NO<sub>2</sub> four moles of •OH are consumed. If the NO<sub>2</sub> are NO<sub>3</sub> are assumed to be produced from reaction of •OH with NO and NO<sub>2</sub> (R13 and R14), production of NO<sub>2</sub> equates to three •OH consumed while NO<sub>3</sub> equates to five •OH. This information is summarized in the Table 3.

Table 3 Assumed hydroxyl radical consumption based on production of measured products

Reaction	•OH utilized per mole
	produced
R10	$H_2O_2 = 2OH$
R17	$CO_2 = 1OH$
R11	O = 2OH
R3	NO = 2OH
R5	$NO_2 = 4OH$
R13	$HNO_2 = 3OH$
R14	$HNO_3 = 5OH$

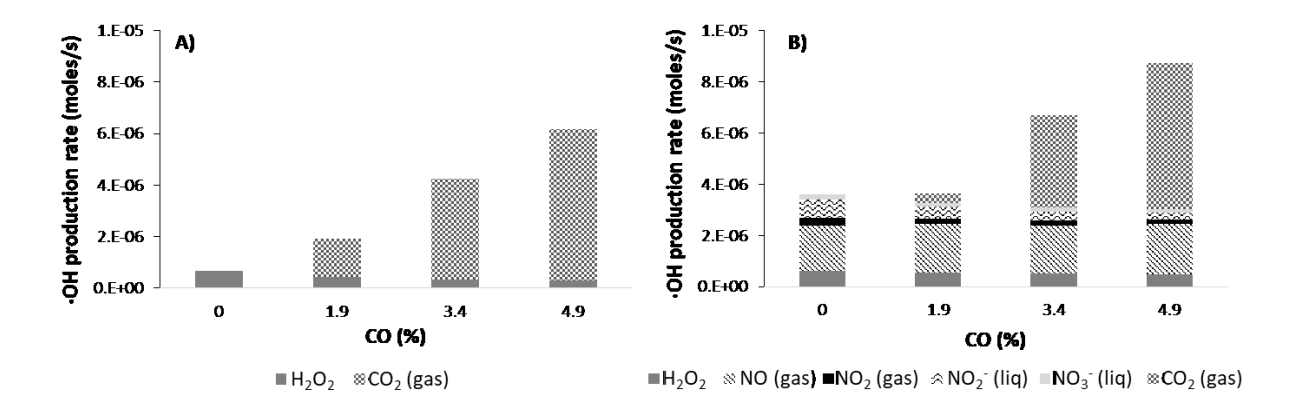
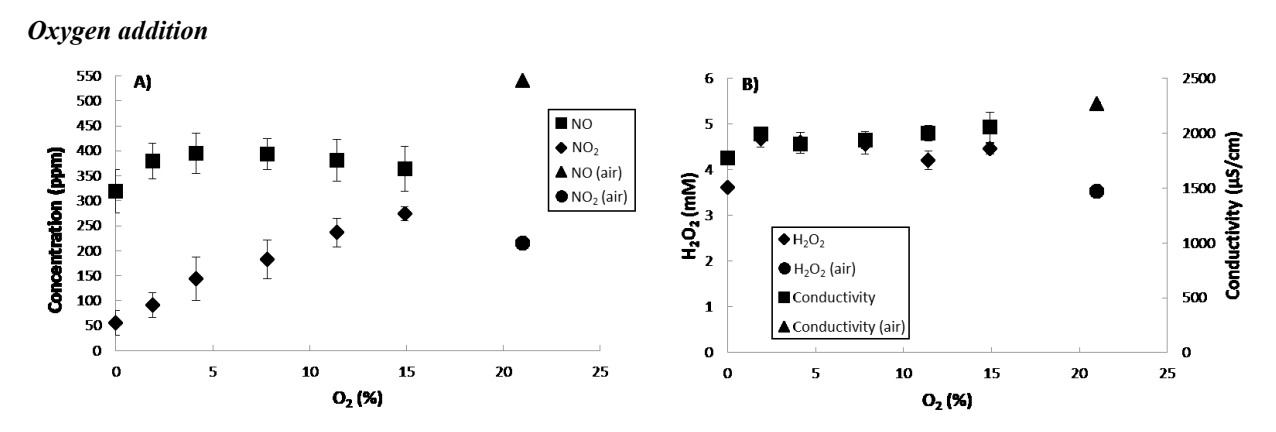


Fig. 11 Estimated hydroxyl radical production rate based on the generation of  $H_2O_2$ ,  $CO_2$ , and nitrogen oxides for various gas mixtures. A) – Ar/CO, B) – 28%  $N_2/Ar/CO$ 

The production rates of •OH based on the assumptions in Table 3 are shown in Figure 11. Figure 11a shows the •OH production rate when only argon was used as the carrier gas with various concentrations of CO added. As the concentration of CO was increased the measured •OH production rate increased significantly while the production rate of  $H_2O_2$  slightly decreased as a result of the •OH scavenging by CO. At 3.4% CO the •OH production rate was  $4 \times 10^{-6}$  moles/s. These results are similar to experiments performed in the same reactor but utilizing a different power supply based upon microsecond pulses where an •OH production rate of  $5 \times 10^{-7}$  moles/s

was found at 2.6% CO [78]. Based on the high production rate of •OH from CO<sub>2</sub> measurements it is clear that significantly more •OH is produced in the system than can be accounted for by H<sub>2</sub>O<sub>2</sub>.

Figure 11b shows the •OH production rate for the 28% N<sub>2</sub>/Ar mixture with various concentrations of CO. The •OH production rate was lower in the case with 1.9% CO in Ar than in the case with 0% CO with 28% N<sub>2</sub> due to the contribution of •OH scavenged by nitrogen oxides. As the CO concentration was increased, •OH production continued to increase up to a value of 8.3x10<sup>-6</sup> moles/s. This result shows that even with the •OH accounted for in the production of nitrogen oxides and H<sub>2</sub>O<sub>2</sub> there is still a significant amount of •OH that remains unutilized (available to react with CO). The energy yield for •OH production can also be calculated by dividing the production rate by the corresponding average discharge power. The highest energy yield was found to be 7x10<sup>-7</sup> moles/J for the case of 28% N<sub>2</sub>/4.9% CO in balance Ar and this value is in close agreement with the value of 5x10<sup>-7</sup> moles/J found in the previous work with microsecond pulses and 2.6% CO in Ar in same reactor [78]. This result suggests that the energy yield in a nanosecond discharge is not significantly different than that of a microsecond discharge; however, it can noted that there are other advantages of the nanosecond power supply, including tolerance of high solution conductivity [63].



**Fig. 12** Chemical analysis of the gas phase (A) and liquid phase (B) for various concentrations of oxygen added to a 28% nitrogen mixture with balance argon. Experimental results for air are also displayed.

To further investigate the role of reactive oxygen species in the process, various concentrations of O<sub>2</sub> (0-15%) were added to the 28% N<sub>2</sub>/Ar mixture. An additional experiment was performed with air. Results for the gas and liquid phase analyses are shown in Figure 12. The only significant change measured with the addition of O<sub>2</sub> was a large increase in NO<sub>2</sub> generation. Because NO is a precursor for NO<sub>2</sub>, it is likely that NO production also increased but it was rapidly converted to NO<sub>2</sub> due to an increased concentration of reactive oxygen species. This would explain the lack of any net change in NO as O<sub>2</sub> concentration was increased. The lack of an increase in conductivity implies that the NO<sub>2</sub><sup>-</sup> and NO<sub>3</sub><sup>-</sup> concentrations did not change with added O<sub>2</sub> and provides further evidence that the conversion of NO and NO<sub>2</sub> into these products is limited by •OH (R13 and R14) and not by other reactive oxygen species.

When air was utilized the results were similar to those with the 15% O<sub>2</sub>, 28% N<sub>2</sub>, balance Ar mixture. Higher concentrations of NO and NO<sub>2</sub> were observed in the gas phase compared to the case with no O<sub>2</sub>; however, little increase was seen in the production of NO<sub>2</sub><sup>-</sup> and NO<sub>3</sub><sup>-</sup>. This result is again consistent with higher atomic oxygen concentrations leading to an increase in NO and NO<sub>2</sub> generation and with a limitation of •OH for further conversion of these products to HNO<sub>2</sub> and HNO<sub>3</sub>. It should also be noted that no O<sub>3</sub> was detected in the gas phase with FTIR for both the O<sub>2</sub> addition and air experiments. This is consistent with other studies with similar plasma conditions where the lack of ozone was attributed to plasma (gas) temperatures above ambient leading to rapid thermal degradation of O<sub>3</sub> [71, 85, 86]. Additionally, any O<sub>3</sub> which could be formed would rapidly react with NO (R6) [26, 27].

#### CONCLUSIONS

Chemical analysis of the products generated when filamentary non-thermal plasma channels propagate along a flowing liquid water film in  $N_2$ /Ar atmosphere shows significant amounts of NO and  $NO_2$  in the gas phase and  $NO_2$ ,  $NO_3$ , and  $H_2O_2$  in the liquid. By inducing chemical quenching of the liquid effluent, this work decouples the chemical reactions induced by the plasma from those which occur in the post-plasma solution. This allows for assessment of the reaction pathways leading to the generation of these chemical species without the complications induced by secondary interactions of the plasma generated molecules. Current work is in progress to develop chemical reaction modeling for further assessment of the reaction pathways described in this paper.

In this work the gas temperature of the plasma channel was found to be approximately 525 K and was unaffected by the  $N_2$  concentration. The electron density was  $7.8 \times 10^{16}$  cm<sup>-3</sup> with no  $N_2$  present (pure Ar) and increased to  $5.6 \times 10^{17}$  cm<sup>-3</sup> at 28%  $N_2$  in Ar. In contrast, the volume (diameter) of the plasma channel decreased with increasing  $N_2$  resulting in a negligible change in total free electrons with  $N_2$  concentration. The production of all nitrogen oxides increased as a function of the amount of  $N_2$  in the feed gas giving a maximum production rate of  $1.5 \times 10^{-6}$  moles/s at an energy yield of 50 eV/molecule at the highest  $N_2$  concentration investigated (28%). The negligible change in total free electrons with  $N_2$  implies that the significant increase in total nitrogen oxides produced with  $N_2$  was mainly caused by an increased availability of nitrogen and not by an increase of free electrons available for reaction.

This work shows that significant generation of nitrogen oxides is possible without a source of oxygen in the feed gas. The reaction of •OH to form water and O (R11) is one likely source of the atomic oxygen needed for NO and NO<sub>2</sub> generation, however, other reactions are possible (R15 and R16). NO formation can then proceed though Reaction 3. However, the addition of oxygen to the gas feed did enhance the overall NOx production by adding an additional atomic oxygen source (R2). •OH does not otherwise appear to directly affect the generation of NO (R12) or NO<sub>2</sub> but does play a key role in the conversion of NO and NO<sub>2</sub> into HNO<sub>2</sub> and HNO<sub>3</sub>, respectively. While further conversion of the remaining gas phase NO and NO<sub>2</sub> into HNO<sub>2</sub> and HNO<sub>3</sub> appears to be limited by •OH, there is still a significant quantity of •OH unutilized as evident from CO scavenging (CO<sub>2</sub> production) and H<sub>2</sub>O<sub>2</sub> production. Future work should be done to investigate capitalizing on this unutilized •OH.

#### **ACKNOWLEDGEMENTS**

This work was supported by the National Science Foundation (CBET 1702166) and Florida State University.

## **APPENDEX**

# Electrical measurements

Temporal alignment of current and voltage probes is essential for accurate analysis of nanosecond discharges. For temporal alignment of these probes the nanopulser was discharged across a resistor placed inside the Rogowski coil while the two voltage probes measured the electrical potential across the resistor. The deskew of each voltage probe was then adjusted to ensure simultaneous rise in each voltage probe with current.

For analysis of the plasma discharge, the high voltage probes were connected across the stainless-steel inlet and outlet capillaries to measure the electric potential across the plasma discharge region. The reactor was placed inside the Rogowski coil so that the discharge region was centered within the coil to measure current flow through the discharge region only. With placement of the voltage and current probes in this fashion, the measured values give the electrical potential between the electrodes and current flow only within the formed plasma channels. More details of the electrical analysis can be found in our previous work [60, 62].

# H<sub>2</sub>O<sub>2</sub> quantification

For  $H_2O_2$  quantification the effluent was discharged directly into a sodium azide solution of sufficient quantity to rapidly remove all  $NO_2$  from the liquid phase. 2 mL of effluent from reactor was discharged into a 1 M sodium azide solution at an equal 1 to 1 volume ratio (i.e. 2 mL sodium azide + 2mL effluent). The  $H_2O_2$  in the resulting solution was then quantified with the  $TiSO_4$  colorimetric method using a UV-Vis spectrometer detailed in our previous publications as well as others (PerkinElmer, Lambda 35) [58, 61, 87]. The resulting concentration was then multiplied by a factor of 2 in order to account for the dilution with the sodium azide solution.

## Nitrate and nitrite quantification

For nitrate and nitrite quantification the pH of the effluent must be rapidly increased to slow/stop the reaction of NO<sub>2</sub><sup>-</sup> with H<sub>2</sub>O<sub>2</sub>. In addition, the solutions were diluted to approximately 10 ppm total nitrogen for protection of the IC instrument. For this procedure, 3 mL of effluent was directly discharged into a 26.7 mL solution of 1 mM NaOH. The pH of the resulting mixture after effluent addition was approximately 10. Calibration curves for the IC were prepared using various dilutions of NaNO<sub>2</sub> and KNO<sub>3</sub>. All samples were analyzed on a Dionex, Aquion ion chromatograph equipped with an IonPac<sup>TM</sup> AS22 column (4 × 250 mm), an AERS<sup>TM</sup> 500 carbonate suppressor, and a conductivity detector. The eluent was 4.5 mM sodium carbonate mixed with 1,4 mM sodium bicarbonate and supplied to the IC system at an isocratic flow of 1.2 mL/min. A sample IC spectrum is shown in Figure 13.

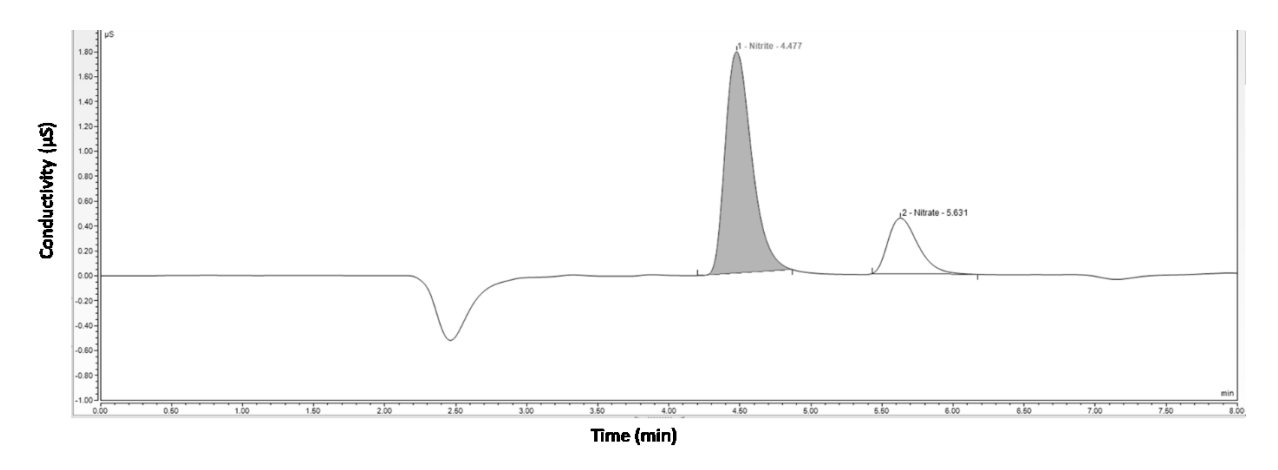


Fig. 13 Sample IC spectrum for 28% N<sub>2</sub> with balance argon as the carrier gas

# NO and NO2 quantification

An FTIR (Jasco – 6700) equipped with a gas flow cell was utilized to analyze the gas phase effluent. Calibration curves for NO and NO<sub>2</sub> were generated by flowing dilutions of 1000 ppm gas standards generated with a mass flow controller (Brooks, 5850E) and balanced with N<sub>2</sub> at the same total flow rate as the experimental conditions (3.4 L/min). For NO the band at 1917.86 cm<sup>-1</sup> was used for quantification while for NO<sub>2</sub> the band at 1637.78 cm<sup>-1</sup> was utilized. The following instrument conditions were used for all FTIR measurements: 8 accumulations, 0.25 cm<sup>-1</sup> resolution, 32 gain, 1.8 mm aperture, and 2 mm/sec scanning speed. Prior to measurements the gas flow cell was purged with N<sub>2</sub> to remove water and air. All measurements were taken after a steady state in the flow cell had been reached by ensuring no change in the intensity of the bands for a period of two minutes. Sample experimental FTIR spectra are shown in Figures 14 and 15.

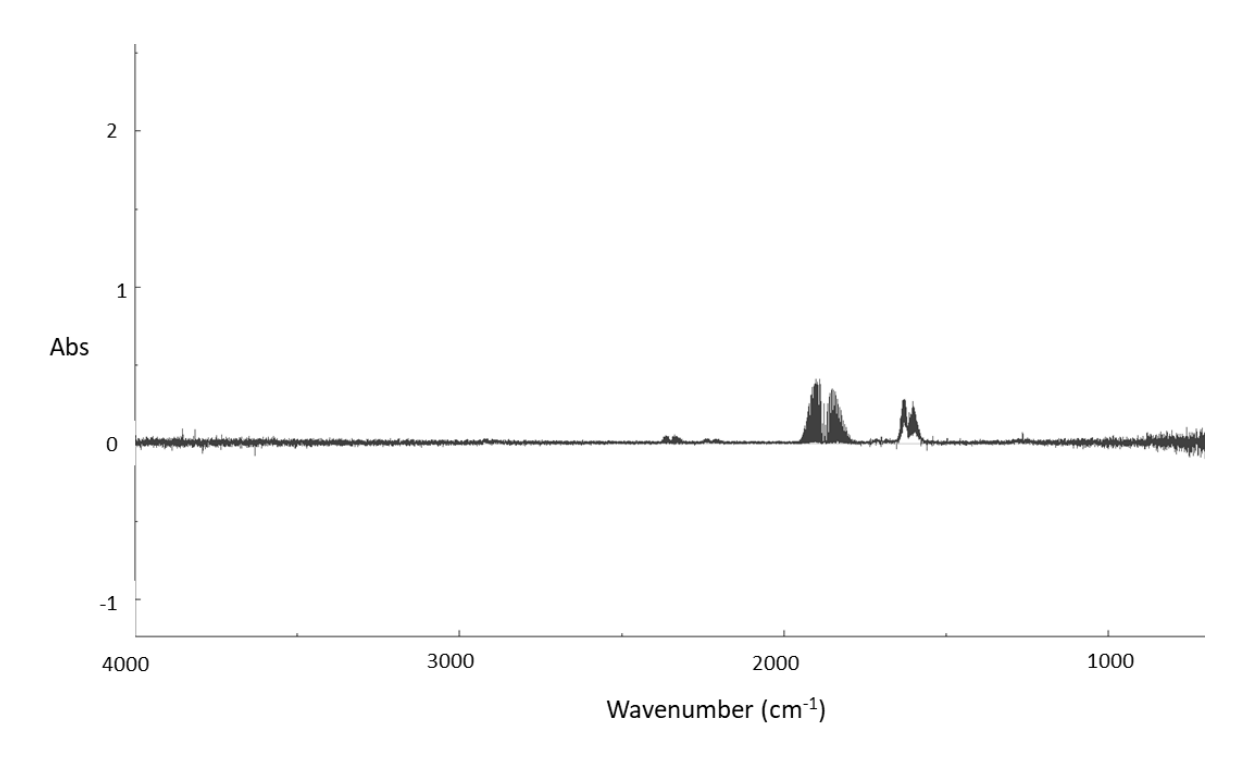


Fig. 14 Sample FTIR spectrum for  $28\%\ N_2$  with balance Ar as the carrier gas

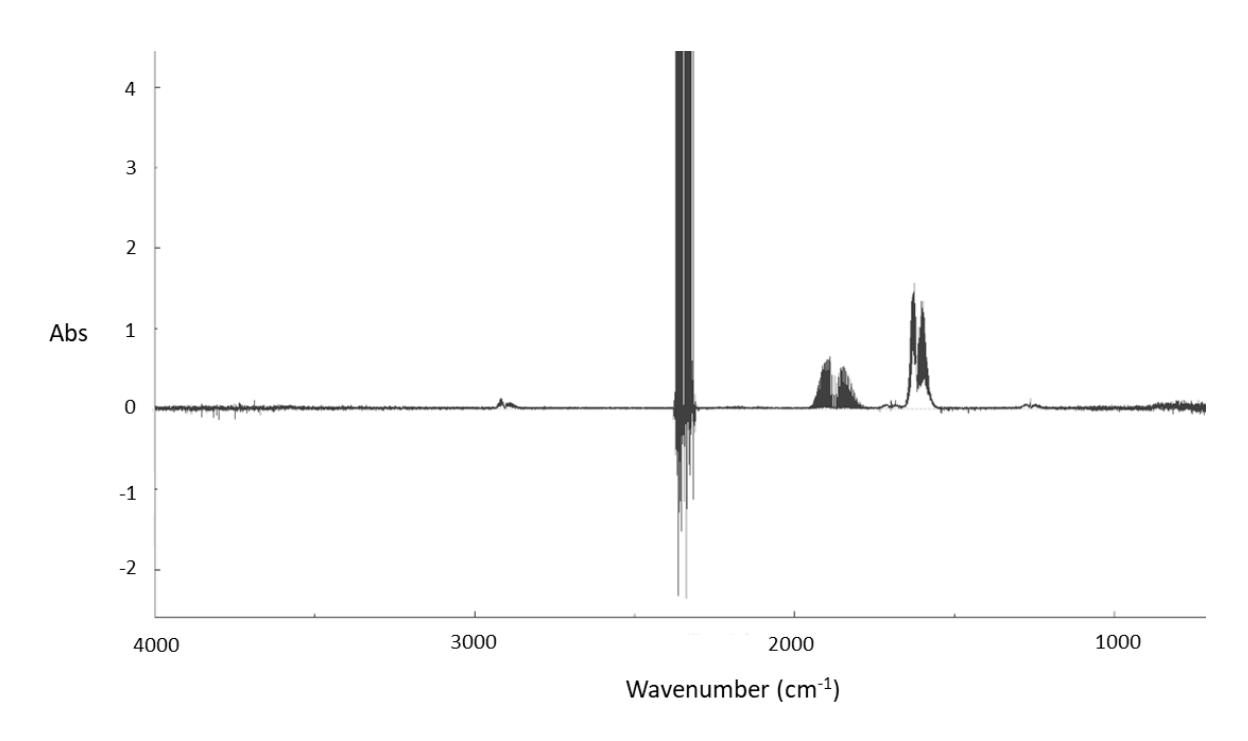
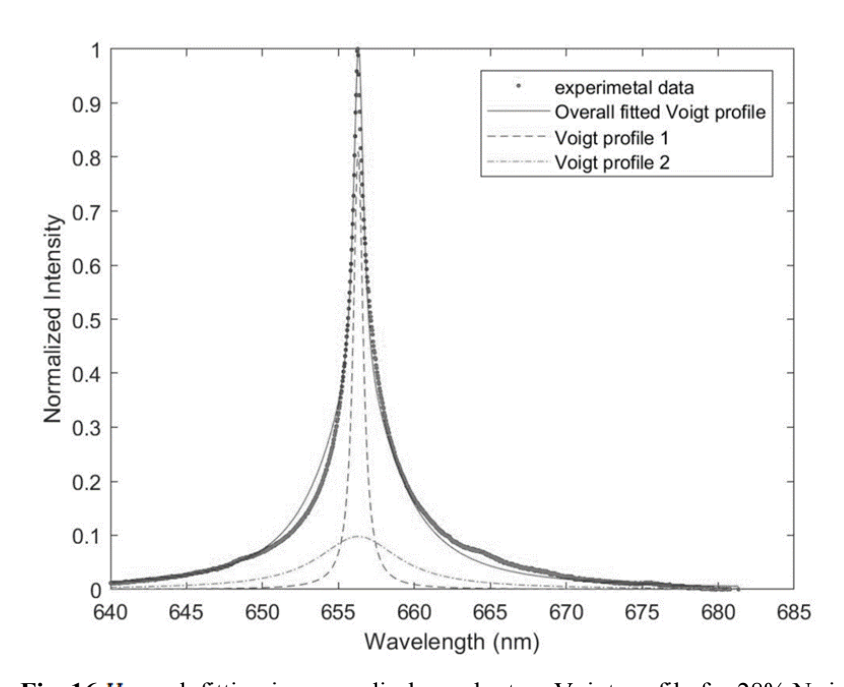


Fig. 15 Sample FTIR spectrum for air as the carrier gas

# **Optical Emission Spectroscopy**

For OES measurements the probe tip was oriented towards the center of the discharge region in as close proximity as possible to the quartz reactor body (approx. 5mm). Stark broadening of the  $H_{\alpha}$  peak was utilized for estimation of the electron density. The  $H_{\alpha}$  peak was observed using an optical emission microscope (Avantes, AvaSpec-ULS3848; wavelength range: 600-700 nm) at 656.3 nm. The  $H_{\alpha}$  peak was deconvoluted into two Voigt profile. The Voigt profile was then deconvoluted into Gaussian and Lorentz profiles. The FWHM of Gaussian profile was determined by Doppler and instrument broadening where Doppler broadening was obtained using gas temperature, and instrumental broadening was obtained by calculating the FWHM of the spectral line with the optical fiber connected to a mercury-argon lamp (Avalight-CAL). The FWHM of the Stark broadening was calculated from the relationship between the FWHM of the Van der Waal's broadening and the FWHM of the Lorentzian profile. More details of this method can be found in a previous publication and a sample of the peak fitting can be found in Figure 16 [63].



**Fig. 16**  $H_{\alpha}$  peak fitting in argon discharge by two Voigt profile for 28% N<sub>2</sub> in argon.

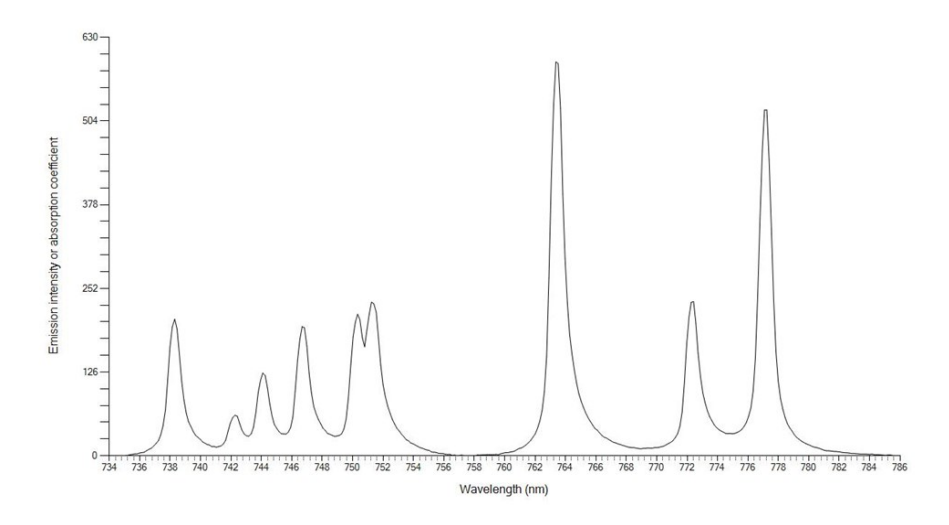


**Fig. 17** Optical emission spectra for 28% nitrogen in argon showing a band at 777 nm which indicates presence of atomic oxygen

## **REFERENCES**

- [1] A. A. Fridman, *Plasma chemistry*, Cambridge; New York: Cambridge University Press, 2008.
- [2] B. R. Locke, P. Lukes, and J. L. Brisset, "Elementary chemical and physical phenomena in electrical discharge plasma in gas-liquid environments and in liquids," *Plasma chemistry and catalysis in gases and liquids*, M. M. V. I. Parvulescu, P. Lukes, ed., Weinheim: Wiley-VCH Verlag GmbH & Co. KGaA, 2012.
- [3] P. Lukes, B. R. Locke, and J. L. Brisset, "Aqueous-phase chemistry of electrical discharge plasma in water and in gas-liquid environments," *Plasma chemistry and catalysis in gases and liquids*, M. M. V. I. Parvulescu, P. Lukes, ed., Weinheim: Wiley-VCH Verlag GmbH & Co. KGaA, 2012.
- [4] B. Patil, Q. Wang, V. Hessel, and J. Lang, "Plasma N2-fixation: 1900–2014," *Catalysis Today*, vol. 256, pp. 49-66, 2015.
- [5] Y. Itikawa, "Cross Sections for Electron Collisions with Oxygen Molecules," *Journal of Physical and Chemical Reference Data*, vol. 38, no. 1, pp. 1-20, 2009.
- [6] L. S. Polak, D. I. Slovetsky, and R. D. Todesaite, *Sov. Phys., High Energy Chemistry*, vol. 9, pp. 142, 1975.
- [7] R. I. Azizov, V. K. Zhivotov, M. F. Krotov, V. D. Rusanov, Y. V. Tarasov, A. A. Fridman, and G. V. Sholin, "Synthesis of Nitrogen Oxides in a Nonequilibrium UHF Discharge Under Electron Cyclotron Resonance Conditions," *Sov. Phys., High Energy Chemistry*, vol. 14, no. 4, pp. 275-277, 1980.
- [8] A. Mizuno, K. Shimizu, A. Chakrabarti, L. Dascalescu, and S. Furuta, "NOX REMOVAL PROCESS USING PULSED DISCHARGE PLASMA," *leee Transactions on Industry Applications*, vol. 31, no. 5, pp. 957-963, Sep-Oct, 1995.

- [9] E. M. vanVeldhuizen, W. R. Rutgers, and V. A. Bityurin, "Energy efficiency of NO removal by pulsed corona discharges," *Plasma Chemistry and Plasma Processing*, vol. 16, no. 2, pp. 227-247, Jun, 1996.
- [10] T. Yamamoto, C. L. Yang, M. R. Beltran, and Z. Kravets, "Plasma-assisted chemical process for NOx control," *Ieee Transactions on Industry Applications*, vol. 36, no. 3, pp. 923-927, May-Jun, 2000.
- [11] Z. H. Wang, B. Li, A. Ehn, Z. W. Sun, Z. S. Li, J. Bood, M. Alden, and K. F. Cen, "Investigation of flue-gas treatment with O-3 injection using NO and NO2 planar laser-induced fluorescence," *Fuel*, vol. 89, no. 9, pp. 2346-2352, Sep, 2010.
- [12] L. W. Huang, and H. Matsuda, "Removal of NO by a pulsed-corona reactor combined with in situ absorption," *Aiche Journal*, vol. 50, no. 11, pp. 2676-2681, Nov, 2004.
- [13] H. Lin, X. Gao, Z. Y. Luo, K. F. Cen, M. X. Pei, and Z. Huang, "Removal of NOx from wet flue gas by corona discharge," *Fuel*, vol. 83, no. 9, pp. 1251-1255, Jun, 2004.
- [14] Y. S. Mok, "Absorption-reduction technique assisted by ozone injection and sodium sulfide for NOx removal from exhaust gas," *Chemical Engineering Journal*, vol. 118, no. 1-2, pp. 63-67, May, 2006.
- [15] Z. H. Wang, J. H. Zhou, J. R. Fan, and K. F. Cen, "Direct numerical simulation of ozone injection technology for NOx control in flue gas," *Energy & Fuels*, vol. 20, no. 6, pp. 2432-2438, Nov, 2006.
- [16] Y. S. Mok, J. H. Kim, I. S. Nam, and S. W. Ham, "Removal of NO and formation of byproducts in a positive-pulsed corona discharge reactor," *Industrial & Engineering Chemistry Research*, vol. 39, no. 10, pp. 3938-3944, Oct, 2000.
- [17] X. D. Hu, G. B. Zhao, S. F. Legowski, and M. Radosz, "Moisture effect on NOx conversion in a nonthermal plasma reactor," *Environmental Engineering Science*, vol. 22, no. 6, pp. 854-869, Nov-Dec, 2005.
- [18] S. E. Yin, B. M. Sun, X. D. Gao, and H. P. Xiao, "The Effect of Oxygen and Water Vapor on Nitric Oxide Conversion with a Dielectric Barrier Discharge Reactor," *Plasma Chemistry and Plasma Processing*, vol. 29, no. 6, pp. 421-431, Dec, 2009.
- [19] M. M. Morgan, M. F. Cuddy, and E. R. Fisher, "Gas-Phase Chemistry in Inductively Coupled Plasmas for NO Removal from Mixed Gas Systems," *Journal of Physical Chemistry A,* vol. 114, no. 4, pp. 1722-1733, Feb, 2010.
- [20] K. Yan, S. Kanazawa, T. Ohkubo, and Y. Nomoto, "Oxidation and reduction processes during NOx removal with corona-induced nonthermal plasma," *Plasma Chemistry and Plasma Processing*, vol. 19, no. 3, pp. 421-443, Sep, 1999.
- [21] D. X. Li, Z. G. Xiao, T. Bin Aftab, and S. H. Xu, "Flue Gas Denitration by Wet Oxidation Absorption Methods: Current Status and Development," *Environmental Engineering Science*.
- [22] I. Jogi, K. Erme, E. Levoll, J. Raud, and E. Stamate, "Plasma and catalyst for the oxidation of NOx," *Plasma Sources Science & Technology,* vol. 27, no. 3, Mar, 2018.
- [23] P. Talebizadeh, M. Babaie, R. Brown, H. Rahimzadeh, Z. Ristovski, and M. Arai, "The role of non-thermal plasma technique in NOx treatment: A review," *Renewable & Sustainable Energy Reviews*, vol. 40, pp. 886-901, Dec, 2014.
- [24] H. H. Kim, "Nonthermal plasma processing for air-pollution control: A historical review, current issues, and future prospects," *Plasma Processes and Polymers*, vol. 1, no. 2, pp. 91-110, Sep 24, 2004.
- [25] F. Beckers, W. Hoeben, A. J. M. Pemen, and E. J. M. van Heesch, "Low-level NOx removal in ambient air by pulsed corona technology," *Journal of Physics D-Applied Physics*, vol. 46, no. 29, pp. 6, Jul, 2013.

- [26] G. B. Zhao, S. V. B. Garikipati, X. D. Hu, M. D. Argyle, and M. Radosz, "Effect of oxygen on nonthermal plasma reactions of nitrogen oxides in nitrogen," *Aiche Journal*, vol. 51, no. 6, pp. 1800-1812, Jun, 2005.
- [27] G. Sathiamoorthy, S. Kalyana, W. C. Finney, R. J. Clark, and B. R. Locke, "Chemical Reaction Kinetics and Reactor Modeling of NOx Removal in a Pulsed Streamer Corona Discharge Reactor," *Industrial and Engineering Chemistry Research*, vol. 38, pp. 1844-1855, 1999.
- [28] T. Huiskamp, W. Hoeben, F. Beckers, E. J. M. van Heesch, and A. J. M. Pemen, "(Sub)nanosecond transient plasma for atmospheric plasma processing experiments: application to ozone generation and NO removal," *Journal of Physics D-Applied Physics*, vol. 50, no. 40, pp. 16, Oct, 2017.
- [29] V. R. Chirumamilla, W. Hoeben, F. Beckers, T. Huiskamp, E. J. M. Van Heesch, and A. J. M. Pemen, "Experimental Investigation on the Effect of a Microsecond Pulse and a Nanosecond Pulse on NO Removal Using a Pulsed DBD with Catalytic Materials," *Plasma Chemistry and Plasma Processing*, vol. 36, no. 2, pp. 487-510, Mar, 2016.
- [30] T. Matsumoto, D. Y. Wang, T. Namihira, and H. Akiyama, "Energy Efficiency Improvement of Nitric Oxide Treatment Using Nanosecond Pulsed Discharge," *Ieee Transactions on Plasma Science*, vol. 38, no. 10, pp. 2639-2643, Oct, 2010.
- [31] T. Matsumoto, D. Wang, T. Namihira, and H. Akiyama, "Process Performances of 2 ns Pulsed Discharge Plasma," *Japanese Journal of Applied Physics*, vol. 50, no. 8, Aug, 2011.
- [32] Y. Itikawa, and N. Mason, "Cross sections for electron collisions with water molecules," *Journal of Physical and Chemical Reference Data*, vol. 34, no. 1, pp. 1-22, 2005.
- [33] J. L. Brisset, A. Doubla, J. Amouroux, M. Goldman, and A. Goldman, "Acid-Base Character of Species Created in a Point-to-Plane Corona Discharge .1. Acid Effect of the Active Changeless Species," *Revue Internationale Des Hautes Temperatures Et Des Refractaires,* vol. 25, no. 4, pp. 229-236, 1989.
- [34] J. L. Brisset, J. Lelievre, A. Doubla, and J. Amouroux, "Interactions with Aqueous Solutions of the Air Corona Products," *Revue de Physique Appliquee*, vol. 25, pp. 535-543, 1990.
- [35] J. Lelievre, N. Dubreuil, and J. L. Brisset, "Electrolysis Processes in D.C. Corona Discharges in Humid Air," *Journal of Physics III France*, vol. 5, pp. 447-457, 1995.
- [36] B. Benstaali, P. Boubert, B. G. Cheron, A. Addou, and J. L. Brisset, "Density and Rotational Temperature Measurements of the OH and NO Radicals Produced by a Gliding Arc in Humid Air," *Plasma Chemistry and Plasma Processing*, vol. 22, no. 4, pp. 553-571, 2002.
- [37] J. L. Brisset, and E. Hnatiuc, "Peroxynitrite: A Re-examination of the Chemical Properties of Non-thermal Discharges Burning in Air Over Aqueous Solutions," *Plasma Chemistry and Plasma Processing*, vol. 32, no. 4, pp. 655-674, Aug, 2012.
- [38] S. Daito, F. Tochikubo, and T. Watanabe, "Improvement of NOx removal efficiency assisted by aqueous-phase reaction in corona discharge," *Japanese Journal of Applied Physics Part 1-Regular Papers Short Notes & Review Papers*, vol. 39, no. 8, pp. 4914-4919, Aug, 2000.
- [39] D. Y. Xie, Y. Sun, T. L. Zhu, and L. Ding, "Removal of NO in Mist by the Combination of Plasma Oxidation and Chemical Absorption," *Energy & Fuels*, vol. 30, no. 6, pp. 5071-5076, Jun, 2016.
- [40] K. Takehana, T. Kuroki, and M. Okubo, "Evaluation on nitrogen oxides and nanoparticle removal and nitrogen monoxide generation using a wet-type nonthermal plasma reactor," *Journal of Physics D-Applied Physics*, vol. 51, no. 20, pp. 11, May, 2018.
- [41] R. Burlica, and B. R. Locke, "Pulsed plasma gliding arc discharges with water spray," *IEEE Transactions on Industry Applications*, vol. 44, no. 2, pp. 482-489, 2008.
- [42] R. Burlica, K. Y. Shih, and B. R. Locke, "Formation of H2 and H2O2 in a Water-Spray Gliding Arc Nonthermal Plasma Reactor," *Industrial & Engineering Chemistry Research*, vol. 49, no. 14, pp. 6342-6349, Jul, 2010.

- [43] R. Wandell, and B. Locke, "Low Power Pulsed Plasma Discharge in a Water Film Reactor," *IEEE Trans. Plasma Sci.*, vol. in press, 2014.
- [44] R. Burlica, M. Kirkpatrick, and B. Locke, "Formation of reactive species in gliding arc discharges with liquid water," *Journal of Electrostatics*, vol. 64, no. 1, pp. 35-43, JAN 2006, 2006.
- [45] J. H. Seinfeld, and S. N. Pandis, *Atmospheric Chemistry and Physics*, New York: John Wiley & Sons, Inc., 1998.
- [46] M. A. Malik, "Nitric Oxide Production by High Voltage Electrical Discharges for Medical Uses: A Review," *Plasma Chemistry and Plasma Processing*, vol. 36, no. 3, pp. 737-766, May, 2016.
- [47] B. S. Patil, F. J. J. Peeters, G. J. van Rooij, J. A. Medrano, F. Gallucci, J. Lang, Q. Wang, and V. Hessel, "Plasma assisted nitrogen oxide production from air: Using pulsed powered gliding arc reactor for a containerized plant," *Aiche Journal*, vol. 64, no. 2, pp. 526-537, Feb, 2018.
- [48] R. Thirumdas, A. Kothakota, U. Annapure, K. Siliveru, R. Blundell, R. Gatt, and V. P. Valdramidis, "Plasma activated water (PAW): Chemistry, physico-chemical properties, applications in food and agriculture," *Trends in Food Science & Technology*, vol. 77, pp. 21-31, Jul, 2018.
- [49] H. Jablonowski, and T. von Woedtke, "Research on plasma medicine-relevant plasma-liquid interaction: What happened in the past five years?," *Clinical Plasma Medicine*, vol. 3, no. 2, pp. 42-52, Dec, 2015.
- [50] N. Cherkasov, A. O. Ibhadon, and P. Fitzpatrick, "A review of the existing and alternative methods for greener nitrogen fixation," *Chemical Engineering and Processing*, vol. 90, pp. 24-33, Apr, 2015.
- [51] Y. He, Z. W. Chen, Z. Li, G. D. Niu, and J. Tang, "Non-thermal plasma fixing of nitrogen into nitrate: solution for renewable electricity storage?," *Frontiers of Optoelectronics*, vol. 11, no. 1, pp. 92-96, Mar, 2018.
- [52] W. Z. Wang, B. Patil, S. Heijkers, V. Hessel, and A. Bogaerts, "Nitrogen Fixation by Gliding Arc Plasma: Better Insight by Chemical Kinetics Modelling," *Chemsuschem*, vol. 10, no. 10, pp. 2145-2157, May, 2017.
- [53] Z. C. Liu, D. X. Liu, C. Chen, D. Li, A. J. Yang, M. Z. Rong, H. L. Chen, and M. G. Kong, "Physicochemical processes in the indirect interaction between surface air plasma and deionized water," *Journal of Physics D-Applied Physics*, vol. 48, no. 49, pp. 20, Dec, 2015.
- [54] D. X. Liu, Z. C. Liu, C. Chen, A. J. Yang, D. Li, M. Z. Rong, H. L. Chen, and M. G. Kong, "Aqueous reactive species induced by a surface air discharge: Heterogeneous mass transfer and liquid chemistry pathways," *Scientific Reports*, vol. 6, Apr, 2016.
- [55] Z. C. Liu, D. X. Liu, C. Chen, Z. J. Liu, A. J. Yang, M. Z. Rong, H. L. Chen, and M. G. Kong, "Post-discharge evolution of reactive species in the water activated by a surface air plasma: a modeling study," *Journal of Physics D-Applied Physics*, vol. 51, no. 17, pp. 12, May, 2018.
- [56] J. L. Brisset, D. Moussa, A. Doubla, E. Hnatiuc, B. Hnatiuc, G. K. Youbi, J. M. Herry, M. Naitali, and M. N. Bellon-Fontaine, "Chemical reactivity of discharges and temporal post-discharges in plasma treatment of aqueous media: Examples of gliding discharge treated solutions," *Industrial & Engineering Chemistry Research*, vol. 47, no. 16, pp. 5761-5781, Aug, 2008.
- [57] J. L. Brisset, and J. Pawlat, "Chemical Effects of Air Plasma Species on Aqueous Solutes in Direct and Delayed Exposure Modes: Discharge, Post-discharge and Plasma Activated Water," *Plasma Chemistry and Plasma Processing*, vol. 36, no. 2, pp. 355-381, Mar, 2016.
- [58] P. Lukes, E. Dolezalova, I. Sisrova, and M. Clupek, "Aqueous-phase chemistry and bactericidal effects from an air discharge plasma in contact with water: evidence for the formation of peroxynitrite through a pseudo-second-order post-discharge reaction of H2O2 and HNO2," *Plasma Sources Science & Technology*, vol. 23, no. 1, pp. 15, Feb, 2014.

- [59] Z. Z. Su, K. Ito, K. Takashima, S. Katsura, K. Onda, and A. Mizuno, "OH Radical Generation by Atmospheric Pressure Pulsed Discharge Plasma and its Quantitative Analysis by Monitoring CO Oxidation," *Journal of Physics D: Applied Physics*, vol. 35, pp. 3192-3198, 2002.
- [60] R. J. Wandell, H. H. Wang, K. Tachibana, B. Makled, and B. R. Locke, "Nanosecond pulsed plasma discharge over a flowing water film: Characterization of hydrodynamics, electrical, and plasma properties and their effect on hydrogen peroxide generation," *Plasma Processes and Polymers*, vol. 15, no. 6, Jun, 2018.
- [61] G. M. Eisenberg, "Colorimetric Determination of Hydrogen Peroxide," *Industrial and Engineering Chemistry Analytical Edition*, vol. 15, no. 5, pp. 327-328, 1943.
- [62] H. H. Wang, R. J. Wandell, and B. R. Locke, "The influence of carrier gas on plasma properties and hydrogen peroxide production in a nanosecond pulsed plasma discharge generated in a water-film plasma reactor," *Journal of Physics D-Applied Physics*, vol. 51, no. 9, pp. 13, Mar, 2018.
- [63] H. Wang, R. Wandell, Tachibana, Kosuke, J. Vorac, and B. Locke, "The Influence of Liquid Conductivity on Electrical Breakdown and Hydrogen Peroxide Production in a Nanosecond Pulsed Plasma Discharge Generated in a Water-film Plasma Reactor," *Journal of Physics D: Applied Physics*, vol. <a href="https://doi.org/10.1088/1361-6463/aaf132">https://doi.org/10.1088/1361-6463/aaf132</a>, 2018.
- [64] J. Vorac, P. Synek, L. Potocnakova, J. Hnilica, and V. Kudrle, "Batch processing of overlapping molecular spectra as a tool for spatio-temporal diagnostics of power modulated microwave plasma jet," *Plasma Sources Science & Technology*, vol. 26, no. 2, pp. 12, Feb, 2017.
- [65] J. Voráč, P. Synek, V. Procházka, and T. Hoder, "State-by-state emission spectra fitting for non-equilibrium plasmas: OH spectra of surface barrier discharge at argon/water interface," arXiv preprint arXiv:1703.09978, 2017.
- [66] A. Y. Nikiforov, C. Leys, M. A. Gonzalez, and J. L. Walsh, "Electron density measurement in atmospheric pressure plasma jets: Stark broadening of hydrogenated and non-hydrogenated lines," *Plasma Sources Science & Technology*, vol. 24, no. 3, pp. 18, May, 2015.
- [67] X. M. Zhu, J. L. Walsh, W. C. Chen, and Y. K. Pu, "Measurement of the temporal evolution of electron density in a nanosecond pulsed argon microplasma: using both Stark broadening and an OES line-ratio method," *Journal of Physics D-Applied Physics*, vol. 45, no. 29, pp. 11, Jul, 2012.
- [68] M. Lieberman, and A. Lichtenberg, *Principles of Plasma Discharge and Materials Processing*, Second Edition ed.: Wiley, 2005.
- [69] G. J. M. Hagelaar, and L. C. Pitchford, "Solving the Boltzmann equation to obtain electron transport coefficients and rate coefficients for fluid models," *Plasma Sources Science & Technology*, vol. 14, no. 4, pp. 722-733, Nov, 2005.
- [70] M. Janda, V. Martisovits, K. Hensel, Z. Machala, and Iop, "Study of transient spark discharge focused at NOx generation for biomedical applications," *Journal of Physics Conference Series*, 2016
- [71] M. Janda, V. Martisovits, K. Hensel, and Z. Machala, "Generation of Antimicrobial NOx by Atmospheric Air Transient Spark Discharge," *Plasma Chemistry and Plasma Processing*, vol. 36, no. 3, pp. 767-781, May, 2016.
- [72] M. Janda, K. Hensel, and Z. Machala, "Kinetic plasma chemistry model of pulsed transient spark discharge in air coupled with nanosecond time-resolved imaging and spectroscopy," *Journal of Physics D-Applied Physics*, vol. 51, no. 33, pp. 10, Aug, 2018.
- [73] B. Tarabova, P. Lukes, M. Janda, K. Hensel, L. Sikurova, and Z. Machala, "Specificity of detection methods of nitrites and ozone in aqueous solutions activated by air plasma," *Plasma Processes and Polymers*, vol. 15, no. 6, pp. 12, Jun, 2018.

- [74] B. R. Locke, and K. Y. Shih, "Review of the methods to form hydrogen peroxide in electrical discharge plasma with liquid water," *Plasma Sources Science & Technology*, vol. 20, no. 3, pp. 15, Jun, 2011.
- [75] B. R. Locke, and S. M. Thagard, "Analysis and Review of Chemical Reactions and Transport Processes in Pulsed Electrical Discharge Plasma Formed Directly in Liquid Water," *Plasma Chemistry and Plasma Processing*, vol. 32, no. 5, pp. 875-917, Oct, 2012.
- [76] S. Mededovic, and B. R. Locke, "Primary chemical reactions in pulsed electrical discharge channels in water," *Journal of Physics D-Applied Physics*, vol. 40, no. 24, pp. 7734-7746, Dec, 2007.
- [77] S. Hofmann, A. F. H. van Gessel, T. Verreycken, and P. Bruggeman, "Power dissipation, gas temperatures and electron densities of cold atmospheric pressure helium and argon RF plasma jets," *Plasma Sources Science & Technology*, vol. 20, no. 6, pp. 12, Dec, 2011.
- [78] K. C. Hsieh, R. J. Wandell, S. Bresch, and B. R. Locke, "Analysis of hydroxyl radical formation in a gas-liquid electrical discharge plasma reactor utilizing liquid and gaseous radical scavengers," *Plasma Processes and Polymers*, vol. 14, no. 8, pp. 14, Aug, 2017.
- [79] A. Lindsay, B. Byrns, W. King, A. Andhvarapou, J. Fields, D. Knappe, W. Fonteno, and S. Shannon, "Fertilization of Radishes, Tomatoes, and Marigolds Using a Large-Volume Atmospheric Glow Discharge," *Plasma Chemistry and Plasma Processing*, vol. 34, no. 6, pp. 1271-1290, Nov, 2014.
- [80] W. J. Bian, X. H. Song, J. W. Shi, and X. L. Yin, "Nitrogen fixed into HNO3 by pulsed high voltage discharge," *Journal of Electrostatics*, vol. 70, no. 3, pp. 317-326, Jun, 2012.
- [81] V. Hessel, A. Anastasopoulou, Q. Wang, G. Kolb, and J. Lang, "Energy, catalyst and reactor considerations for (near)-industrial plasma processing and learning for nitrogen-fixation reactions," *Catalysis Today*, vol. 211, pp. 9-28, Aug, 2013.
- [82] B. T. J. van Ham, S. Hofmann, R. Brandenburg, and P. J. Bruggeman, "In situ absolute air, O-3 and NO densities in the effluent of a cold RF argon atmospheric pressure plasma jet obtained by molecular beam mass spectrometry," *Journal of Physics D-Applied Physics*, vol. 47, no. 22, pp. 9, Jun, 2014.
- [83] D. P. Park, K. Davis, S. Gilani, C. A. Alonzo, D. Dobrynin, G. Friedman, A. Fridman, A. Rabinovich, and G. Fridman, "Reactive nitrogen species produced in water by non-equilibrium plasma increase plant growth rate and nutritional yield," *Current Applied Physics*, vol. 13, pp. S19-S29, Mar, 2013.
- [84] Z. Z. Su, K. Ito, K. Takashima, S. Katsura, K. Onda, and A. Mizuno, "OH radical generation by atmospheric pressure pulsed discharge plasma and its quantitative analysis by monitoring CO oxidation," *Journal of Physics D-Applied Physics*, vol. 35, no. 24, pp. 3192-3198, Dec, 2002.
- [85] X. L. Tang, J. G. Wang, H. H. Yi, S. Z. Zhao, F. Y. Gao, and C. Chu, "Nitrogen Fixation and NO Conversion using Dielectric Barrier Discharge Reactor: Identification and Evolution of Products," *Plasma Chemistry and Plasma Processing*, vol. 38, no. 3, pp. 485-501, May, 2018.
- [86] M. J. Pavlovich, T. Ono, C. Galleher, B. Curtis, D. S. Clark, Z. Machala, and D. B. Graves, "Air spark-like plasma source for antimicrobial NOx generation," *Journal of Physics D-Applied Physics*, vol. 47, no. 50, pp. 10, Dec, 2014.
- [87] R. J. Wandell, S. Bresch, K. Hsieh, I. V. Alabugin, and B. R. Locke, "Formation of Alcohols and Carbonyl Compounds from Hexane and Cyclohexane With Water in a Liquid Film Plasma Reactor," *Ieee Transactions on Plasma Science*, vol. 42, no. 5, pp. 1195-1205, May, 2014.